Catena 174 (2019) 452–468

Contents lists available at ScienceDirect

Catena

journal homepage: www.elsevier.com/locate/catena

Deconstructing aeolian landscapes

Patrick Barrineau[a,*], Iliyana Dobreva[a,b], Michael P. Bishop[a,b], Chris Houser[c], Steven L. Forman[d]

[a] Texas A&M University, Dept. of Geography, College Station, TX 77843, United States of America
[b] Texas A&M University, Center for Geospatial Sciences, Applications & Technology, College Station, TX 77843, United States of America
[c] University of Windsor, Dept. of Earth and Environmental Sciences, Windsor, ON N9B 3P4, Canada
[d] Baylor University, Dept. of Geosciences, Waco, TX 76798, United States of America

ARTICLE INFO

Keywords:
Great Plains
Optically simulated luminescence dating (OSL)
Dune system evolution

ABSTRACT

Semi-stabilized dune systems are important indicators of Quaternary drought variability across central North America. The South Texas sand sheet (STSS) is the southernmost relict dune system on the Great Plains, and is exposed to higher evapotranspiration and moisture variability than similar landscapes farther north. In this study, a combination of surface and sub-surface remote sensing is used to analyze the semi-stabilized dune landscapes of the STSS in order to delineate distinct aeolian sediments that can represent generations of sedimentation or particular climate conditions. The combination of multi-resolution analysis of a LiDAR dataset, electromagnetic conductivity surveys, and XRF scans of soil cores are shown to be useful tools for deconstructing and modeling the environmental history of the STSS. Optically-stimulated luminescence (OSL) dating of identified surfaces suggests that the STSS is older than previously thought. Since dune systems are excellent repositories of climate and biophysical data for a landscape, and are also sensitive to changes in climate and ecology, the methodology employed in this study can be used to characterize the vulnerability of other similar environments to climate change through the Holocene and over the next century.

1. Introduction

Across the Great Plains of the United States and Canada there are relict dune systems associated with periodic drying throughout the Holocene (e.g. Loope and Swinehart, 2000; Mason et al., 2004; Cordova et al., 2005; Hugenholtz and Wolfe, 2005a; Lepper and Scott, 2005; Houser et al., 2015; Barrineau et al., 2016). These systems have an abundance of sand and silt-sized sediment and are consistently exposed to winds above threshold velocity for aeolian transport (Forman et al., 2009; Halfen and Johnson, 2013). With less moisture expected across much of North America through the 21st century, understanding the scale and nature of these systems' reactions to climate change and other external forcings will be valuable knowledge while navigating a new American drought landscape (Albrecht, 1988; Kettle et al., 2007; Kustu et al., 2010; Hugenholtz et al., 2012; Halfen and Johnson, 2013; Brena-Naranjo et al., 2014; Cook et al., 2016).

Active, migrating dunes can persist through both arid and humid periods. So, the transition between vegetated and dune landscapes often drives system-wide evolution in topography, ecology, and hydrology (see Wolfe and Nickling, 1993; Hugenholtz and Wolfe, 2005b; Baas and Nield, 2010). Piecing together localized histories of activation and stabilization aids understanding how these systems responded to past events (e.g., Woodhouse and Overpeck, 1998; Hugenholtz and Wolfe, 2005a; Sridhar et al., 2006; Xiadong et al., 2007; Singhvi and Porat, 2008; Mason et al., 2009), and how they may react to future changes (Muhs and Holliday, 1995; Thomas et al., 2005; Thomas and Wiggs, 2008; Thorpe et al., 2008; Ashkenazy et al., 2012; Bhattachan et al., 2014). Complex activation histories of dune systems are typically derived from age-dated sediments (see Forman et al., 2009), paleosols and sedimentary facies analyses, or previous studies (see Forman et al., 2001; Hugenholtz et al., 2012; Halfen and Johnson, 2013).

Current approaches to studying relict dune systems can introduce a selection bias in sampling age-dated sediments (see Halfen and Johnson, 2013; Barrineau et al., 2016). Sample collection and laboratory procedures for luminescence dating are expensive and time consuming, limiting most researchers from taking more than a handful of samples. Halfen and Johnson (2013) estimate there are ~800 dated samples of Great Plains dune systems, covering an area of $> 1 \times 10^7$ km and spanning ~6000 years of environmental history. This distribution of samples skews regional interpretations of dune activity; the Nebraska Sand Hills alone account for nearly 50% of the published dates available between Kansas and Alberta (see Halfen and Johnson, 2013). There may be considerable portions of known aeolian systems that remain under-sampled, or that there are systems that remain

* Corresponding author.
E-mail address: patrick@coastalscience.com (P. Barrineau).

https://doi.org/10.1016/j.catena.2018.11.038
Received 3 January 2018; Received in revised form 20 November 2018; Accepted 24 November 2018
Available online 04 December 2018
0341-8162/ © 2018 Elsevier B.V. All rights reserved.

undocumented. Improved delineation of surface and sub-surface sediments provides a more accurate idea of where sampling is taking place and how and if those sites are representative of changes across the landscape.

This study uses a combination of topographic, geophysical, and sedimentological data to delineate aeolian landforms and sediments in South Texas that can represent generations of sedimentation or climate conditions (see Kocurek and Ewing, 2005; Ewing et al., 2015; Barrineau et al., 2016). Principal Components Analysis (PCA), performed on a LiDAR-generated elevation model, helps to delineate distinct aeolian morphologies (see Ewing et al., 2015; Barrineau et al., 2016). Using the PCA results as a guide, an electromagnetic induction (EMI) survey is performed to determine the relationship between surface forms and sub-surface moisture and soil patterns. Finally, samples are dated using the optically-stimulated luminescence (OSL) technique. Results of the PCA and EMI analyses are qualitatively comparable to published soil maps, and OSL dates from specific soil series begin to shed light on how different soil series can be associated with distinct dune activation periods. The findings demonstrate these techniques can be deployed across a relatively large area, collect continuous data series, and be used to generate visualizations and conceptual models of stabilized aeolian landscape evolution. With the addition of dated samples, it is possible to begin constructing a conceptual model of periodic dune activations for the system.

2. Study site

The South Texas Sand Sheet (STSS) is an extension of the West Gulf Coastal Prairie (EPA Level III No. 34; Omernik and Griffith, 2014) that lies across over 8000 km^2 between Corpus Christi and the Rio Grande (Fig. 1; Griffith et al., 2004). The study area processed using the PCA is roughly half the total area of the STSS, and the sub-area sampled for OSL analysis in this manuscript measures roughly 50 km^2 and is located along a gradient between different soils, topography, and vegetation communities. Winds across the STSS are annually bimodal, with a dominant southeasterly flow during summer and a secondary northwesterly flow during winter (Norwine and Bingham, 1987). The southeasterly winds flow across the shallow, hypersaline Laguna Madre estuary, which is often blown dry and is a major transport pathway for wind-blown sediment from Padre Island to the STSS. Sediments across the study area are uniformly aeolian with little to no recognized sedimentary structures (Haile and Brezina, 2012; Forman et al., 2009). There is a change from sub-humid to semi-arid climates such that annual rainfall decreases from over 800 mm to < 600 mm in a span of < 80 km across the STSS. This average difference is inherited from the inter-annual variability in rainfall across the region, through which consecutive years may see upwards of a half meter difference in total precipitation (Johnston, 1963; Diamond and Fulbright, 1990).

Activations in the STSS discussed herein are correlated with the previous chronology published from the study region (Forman et al., 2009) and may be associated with widespread regional drought across the Southern Plains in New Mexico, Texas, and Oklahoma (Grissino-Mayer, 1996; Holliday, 1997; Frederick, 1998; Hall and Penner, 2012). In this respect, it is quite like many of the relict dune systems farther north. However, there are two important distinctive qualities of the STSS that make it valuable to scientific investigation. First, as it is near the southernmost extension of the Great Plains the STSS is exposed to higher potential evapotranspiration rates than other similar relict aeolian landscape (Norwine et al., 1978; LeHouerou and Norwine, 1987; Norwine and Bingham, 1987; Yu et al., 2006). Second, the STSS and surrounding areas were inhabited as early as the 17th century and explored by Spanish and Mexican settlers who kept detailed notes on the ecology and morphology of the region – earlier than many similar systems in Nebraska, the Dakotas, or the Canadian Prairie. As a result, there are historical records of various system states that may be qualitatively compared to modern conditions. These include the diaries of General Manuel de Mier y Terán and botanist Jean Louis Berlandier (see O'Shea, 1935; Berlandier, 1980; Jackson, 2000).

The sandy substrate in the STSS alters vegetation communities from the adjacent coastal tallgrass prairies like the Nebraska Sand Hills (Smeins et al., 1991; Fulbright et al., 1990). Soils across the South Texas sand sheet are highly variable, and reflect previous dune activity as well as ecological succession (Diamond and Fulbright, 1990; Fulbright et al., 1993). Vegetation assemblages across the STSS include tallgrass prairie, sparse sandy grasslands, shallow wetlands, and dense groves of live oak (*Quercus virginiana*) and honey mesquite (*Prosopis glandulosa*) known as 'mottes' (Fulbright et al., 1990). Under humid conditions dense, mature stands of oak motte stop nearly all wind energy from reaching the ground surface (Diamond and Fulbright, 1990; Smeins et al., 1991; Fulbright et al., 1993). Across the landscape, unimpeded ground-level winds often exceed threshold shear velocities for sand transport (Yu et al., 2006). As a result, across the system there are migrating dune patches interspersed among a mixture of otherwise-robust woodlands and shrublands. The distribution of wind-blown sands versus finer clay lenses (often indicating an inter-dune surface) in the shallow subsurface is related to previous dune activity, and can affect vegetation development for decades following activation or stabilization (F. Smeins, pers. comm., 2014; Fulbright et al., 1993; Diamond and Fulbright, 1990).

In the only published sedimentological analysis from the STSS, historic dune activity was dated at roughly 100 yr, 200 yr, 2000 yr, and 2700 yr (Forman et al., 2009). The most recent activation may be climate driven and related to a series of droughts in the first half of the twentieth century, while the penultimate activation may correspond to enhanced aridity during 1789–1790 CE (PDSI −3.8 and −4.7; Cook and Krusic, 2004; Yu et al., 2006; Forman et al., 2009). Early settlement of the region and the introduction of livestock may have also influenced the activation of dune systems during the 18th century, though this is difficult to confirm (Johnston, 1963; Fulbright et al., 1993; Forman et al., 2009). The older activations are associated with regional drought in the Southern High Plains of Texas and New Mexico as well as South Texas, which suggests a regional climatic control on large-scale dune activation (Cook et al., 2004; Yu et al., 2006; Miao et al., 2004; Forman et al., 2009).

3. Methods

3.1. Digital elevation model

The LiDAR data were collected in 2009 as part of the National Elevation Dataset (NED) program. A digital elevation model was derived from raw point clouds with a cell size of 3 × 3 m for our study area, which covers roughly half of the sand sheet. Multi-resolution analysis was used to generate 21 DEMs from the original elevation model representing different spatial resolutions. A Gaussian filter was used to calculate average altitudes at each pixel using intervals designed to capture scale-dependent topographic variation across the study area resulting from different phases of aeolian activity. A 5-m interval was used out to 30 m, and a 30-m interval was used from 30 to 480 m for each grid cell location. The larger interval was used to measure differences in morphology at a dune patch scale, while the smaller interval was used to identify changes within individual bedforms. This way smaller-scale variations that influence wind flow and the migration patterns of active dunes are weighted as much as larger- and longer-scale variations. Each successive Gaussian filter progressively represents more generalization with respect to the true elevation value (e.g., Filter 1 = 5 m radius, Filter 2 = 10 m radius…Filter 6 = 30 m radius, Filter 7 = 60 m radius…Filter 22 = 480 m radius).

3.2. Principal Components Analysis (PCA)

PCA is commonly used to reduce large data sets based upon the

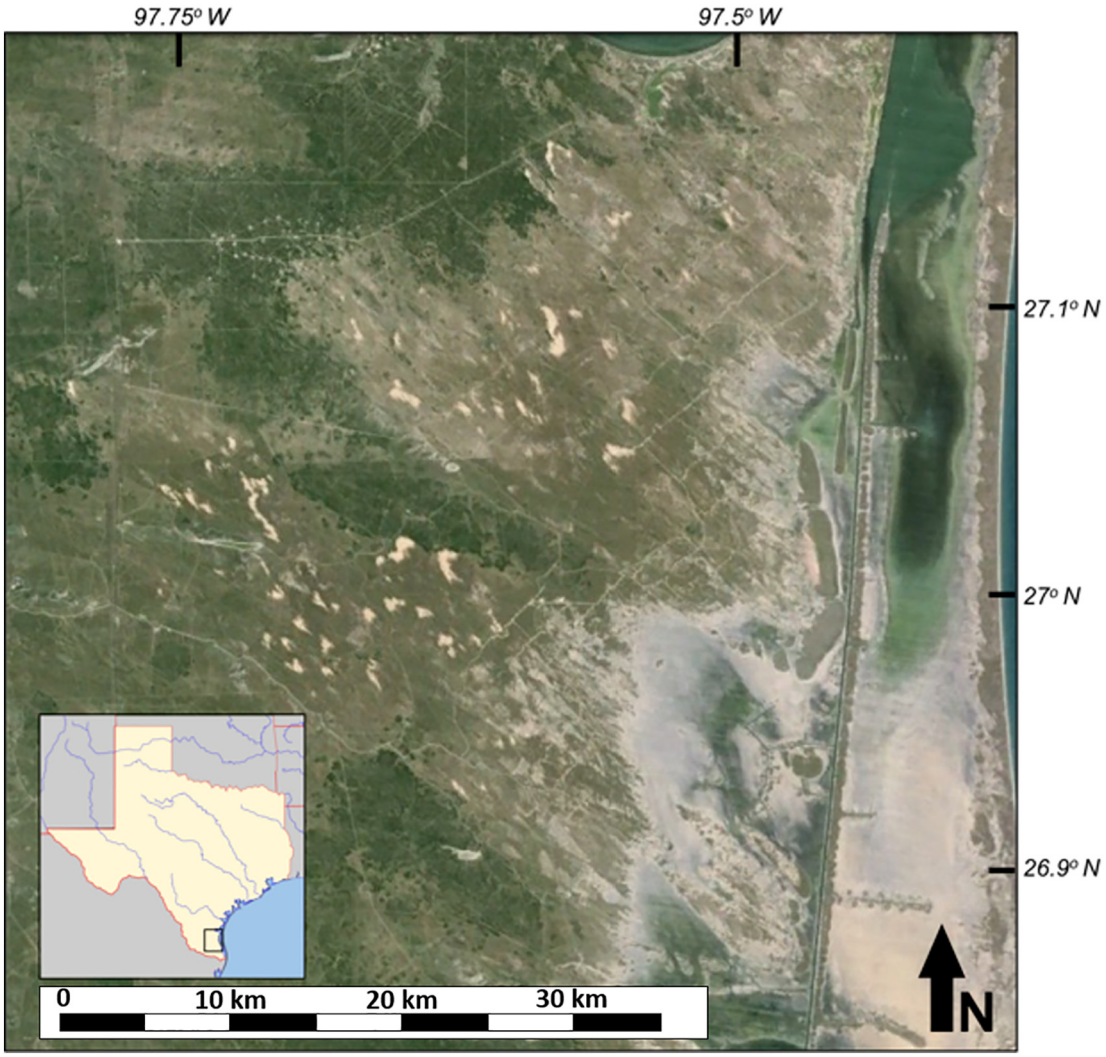

Fig. 1. Study region visible image with location in Texas shown in inset.

degree of multicollinearity, such that it isolates or extracts the significant linear variance components from the dataset (Jensen, 2005). PCA has been used with satellite imagery (Fung and LeDrew, 1987; Rodarmel and Shan, 2002) and RADAR (Grunsky, 2002; Guitet et al., 2013) to assess variations in vegetation cover and mineralogy, to analyze topographic variations characteristic of distinct process-form regimes (Wright et al., 1985; Plant and Griggs, 1992; Kuriyama and Lee, 2001; Houser et al., 2008; Houser and Hamilton, 2009), and with seismic data to identify distinct strata (Guo et al., 2009; Coleou et al., 2003). However, geomorphological studies using PCA for analyzing multi-resolution datasets are rare, as multi-resolution data are not routinely generated, and software may not be readily available. By improving upon previous multi-resolution analyses from this landscape (Barrineau et al., 2016) and comparing the PCA output to field-collected soil cores, this study offers a more robust assessment of this methodology in semi-stabilized aeolian environments.

The multi-resolution dataset was analyzed using unstandardized PCA based upon the covariance matrix, and produced a series eigenvalues and eigenvectors. Eigenvalues describe the variance structure of each component with respect to the total variance of the multi-resolution dataset (i.e., how much variance each component represents). A higher eigenvalue of one component versus another indicates more variance within the dataset is included in that component. Eigenvectors represent the coefficients that are used to transform the multi-resolution dataset into components, and they describe the contribution of variance from a portion of the data set to each component (in this case, at spatial scales). Eigenvector values are relative to where within the data-space variance is weighing heavily on a component. In this respect, each component generates one eigenvalue indicating how much of the original dataset's variance is incorporated into each component, and many eigenvectors indicating where in the original dataset a component is more heavily weighted. After generating the components, an unsupervised k-means algorithm was used to generate a 4-way classification that provides a more discrete visualization of distinct morphometries.

3.3. X-Ray Fluorescence (XRF) scanning

XRF core scanning is a useful technique for investigating geochemical properties of soil samples measured in profile down the soil column. Samples are exposed to X-radiation, causing electrons to be ejected from inner atomic shells. Electrons from the outer shells fill these vacancies and emit a pulse of X-radiation (Jenkins and DeVries, 1970). The energy and wavelength spectra of this emission, which vary based upon the element, are measured and an estimation of elemental concentrations results. XRF analysis requires samples to be prepared before laboratory testing and made as homogeneous and smooth as possible. Because split cores will always contain variation in grain size, moisture, and shape, these conditions are incompatible with the reality of analyzing field-collected core samples. Moreover, the results will

Fig. 2. Locations of 10 core samples collected across the study area.

always be affected by the space between the scanner and core because X-radiation excited by the XRF system will compromise the measurement of many light elements (see Rothwell and Rack, 2006). Despite these weaknesses, XRF is widely regarded as for measuring soil properties as a function of historical changes in biophysical parameters (Andres et al., 2003; Haug et al., 2003; Rothwell and Rack, 2006; Darrénougué et al., 2009).

XRF analysis was performed on split cores in the Integrated Ocean Discovery Program (IODP) laboratory at Texas A&M University using a third-generation Avaatech XRF Core Scanner. Cores were split, separated, and sampled at 1 cm intervals. Excitation was performed at 10 and 30 kV, and measured elemental intensities for major elements between Al and U. The output data were not calibrated to derive elemental concentrations. Because this study uses XRF analysis to qualitatively assess the local accuracy of soil surveys, and identify specific soil series across the study area, elemental intensities are sufficient (see Rothwell and Rack, 2006, and Weltje and Tjallingii, 2008).

To associate apparent conductivities with in situ conditions of grain size and soil series, two soil cores were placed within the small study area in this study as part of a larger survey of ten cores. Using the results of Barrineau et al. (2016) and Natural Resource Conservation Service (NRCS; Haile and Brezina, 2012) soil surveys to select sampling sites, cores were collected during the summer of 2015. The locations of these samples were chosen specifically to maximize the amount of contextual information on aeolian soils by sampling within a mixture of subdued and dramatic aeolian topographies. Cores 5 and 6, used here, were placed on either side of an actively migrating dune patch in the central STSS.

3.4. Electromagnetic induction (EMI) survey

Traditional EMI sensors consist of separate transmitter (TX) and receiver (RX) coils connected by cables, placed at a specific distance apart (or offset). This offset is important because it determines the depth at which a portion of the subsurface may be measured. The frequency at which traditional EMI profilers measured electromagnetic properties was commonly fixed and the depth of measurements was controlled by offset. So, EMI data are often interpreted via analysis of a single frequency (Huang and Won, 2000). With newer portable EMI profilers, the offset is fixed by physically connecting the TX and RX coils into a single lightweight instrument that may be carried by a single individual. Because the offset in newer profilers is fixed, these profilers instead collect data at multiple frequencies designed to penetrate the surface to different depths and collect electromagnetic information. Lower frequencies result in less subsurface attenuation than higher frequencies, so there is an inverse relationship between frequency and depth of measurement.

This study uses a GSSI Profiler EMP 400™ that is capable of measuring conductivity at multiple frequencies ranging from 1 to 16 kHz, with a 1 kHz increment and an offset of 1.21 m (Huang and Rudd, 2008). Surveys were collected over 2 days during October 2014 at 3, 5, and 15 kHz frequencies to measure conductivity within ~1–2 m of the surface (e.g., 15 kHz) and at 3–4 m beneath the surface (e.g., 3 and 5 kHz). These data were collected along a series of 6 transects at 10 m intervals spaced 50 m apart from one another, with a seventh transect connecting all others. The lower frequencies were specifically selected to bracket a nonconformity in the subsurface of the study site, which previous research suggests occurs at around 3 m beneath the surface

Table 1
Optically stimulated luminescence (OSL) ages on quartz grains from aeolian deposits South Texas Sand Sheet, Kennedy Ranch, Texas.

locality/core/depth (cm)	Lab number	Aliquots[a]	Grain Size (μm)	Finite mix/central Equivalent dose (Gray)[b]	Over-dispersion (%)[c]	U (ppm)[d]	Th (ppm)[d]	K (%)[d]	Cosmic dose rate (mGray/yr)	Dose rate (mGray/yr)[e]	Finite mix or central model OSL age (yr)[f]
Kennedy Ranch/5/15	BG4108	33/35	250–150	0.16 ± 0.01[g]	40 ± 5	1.08 ± 0.01	2.66 ± 0.01	1.51 ± 0.01	0.19 ± 0.02	2.03 ± 0.10	75 ± 7
Kennedy Ranch/5/100	BG4109	35/35	250–150	7.19 ± 0.31	18 ± 2	0.93 ± 0.01	1.94 ± 0.01	1.33 ± 0.01	0.17 ± 0.02	1.74 ± 0.09	4135 ± 300
Kennedy Ranch/8/15	BG4106	34/35	250–150	0.41 ± 0.02[g]	51 ± 6	0.79 ± 0.01	1.73 ± 0.01	1.32 ± 0.01	0.19 ± 0.02	1.70 ± 0.09	235 ± 20
Kennedy Ranch/8/105	BG4107	34/35	250–150	3.19 ± 0.13	16 ± 2	0.73 ± 0.01	1.68 ± 0.01	1.30 ± 0.01	0.17 ± 0.02	1.64 ± 0.08	1935 ± 140
Kennedy Ranch/10/35	BG4110	33/34	250–150	0.40 ± 0.03[g]	60 ± 7	0.77 ± 0.01	1.89 ± 0.01	1.30 ± 0.01	0.19 ± 0.02	1.68 ± 0.09	230 ± 25
Kennedy Ranch/10/95	BG4111	34/36	250–150	11.67 ± 0.43	13 ± 2	0.81 ± 0.01	2.52 ± 0.01	1.36 ± 0.01	0.17 ± 0.02	1.78 ± 0.09	6560 ± 460

[a] Aliquots used in equivalent dose calculations versus original aliquots measured.
[b] Equivalent dose calculated on a pure quartz fraction with about 10–50 grains/aliquot and analyzed under blue-light excitation (470 ± 20 nm) by single aliquot regeneration protocols (Murray and Wintle, 2003). The central age model of Galbraith et al. (1999) was used to calculated equivalent dose when overdispersion values are < 20% (at one sigma errors); a finite mixture or minimum age model (Galbraith and Green, 1990) was used with overdispersion values > 20% to determine the youngest equivalent dose population.
[c] Values reflect precision beyond instrumental errors; values of ≤20% (at 1 sigma limit) indicate low dispersion in equivalent dose values and an unimodal distribution.
[d] U, Th and K content analyzed by inductively-coupled plasma-mass spectrometry analyzed by ALS Laboratories, Reno, NV; U content includes Rb equivalent. Includes also a cosmic dose rate calculated from parameters in Prescott and Hutton (1994).
[e] Assumes a moisture content of 3 ± 1%.
[f] Systematic and random errors calculated in a quadrature at one standard deviation. Datum year is 2010 CE.
[g] Equivalent dose by the Minimum Age Model (Galbraith et al., 1999) are nearly identical at 0.16 ± 0.01 Gy (BG4108), 0.40 ± 0.03 Gy (BG4106) and 0.38 ± 0.04 Gy (BG4110) to values by the FMM and serves as a test of precision.

(Diamond and Fulbright, 1990; Fulbright et al., 1993; Forman et al., 2009). The profiler is controlled by a wireless Bluetooth™ interface incorporated into a TDS RECON-400 Personal Digital Assistant (PDA). GPS coordinates are recorded at each measurement location with a positional accuracy of ~1 m.

3.5. Field-collected cores

Ten soil cores were collected to associate subsurface conditions with morphometry, and verify publicly-available soils data indicating the distribution of soil orders of different ages around the study area (Fig. 2). Using the results of Barrineau et al. (2016) and soil surveys of the Natural Resource Conservation Service (NRCS; Haile and Brezina, 2012), sampling sites were arranged to capture multiple distinct environments of the STSS and cores were collected during the summer of 2015. The locations of these samples were chosen specifically to maximize the amount of historical information on aeolian activation by sampling within a mixture of older and younger aeolian landforms. Because of budget limitations, only certain cores could be dated using OSL; however, every core was photographed, sampled for grain size statistics, and scanned for XRF. Seven of the ten cores (Cores 1, 2, 5, 6, 8, 9, 10) are featured in this analysis.

Cores 1 and 2 were collected along a topographic gradient, placed specifically to test the ability of multi-resolution PCA to discretize small-scale changes in morphometry (Focus Area 1). Cores 5 and 10 were collected away from active or recently active dunes, but at locations that the PCA output identified as being characteristically aeolian (Focus Area 2). Cores 9 and 6 were collected in areas with hummocky topography and relatively immature prairie vegetation communities (Focus Area 3). Using a space for time substitution, Cores 5 and 8 are the representative members of soil characteristics on the upwind and downwind margins of actively migrating dune systems. Core 10 is used as a representative sample of much older sediments with little evidence for recent dune activity.

The collected cores range in depth from 90 cm to 150 cm, and were collected manually using a sledgehammer, post hole diggers, and a PVC pipe housing. XRF analysis was performed on split cores in the Integrated Ocean Discovery Program (IODP) laboratory at Texas A&M University using a third-generation Avaatech XRF Core Scanner. Cores were split, separated, and sampled at 1 cm intervals. Excitation was performed at 10 and 30 kV, and measured elemental intensities for major elements between Al and U. Grain size measurements were collected in the laboratory using a Horiba Camsizer (www.horiba.com), which digitally images and analyzes thousands of particles for each sample. Samples were collected from split cores at 10 cm intervals and run through the camsizer for 5 min each. Detection limits for the camsizer were selected from Wentworth scale grain sizes, ranging from 0.063–0.5 mm, and distributions were collected at 10th, 50th, and 90th percentiles.

3.6. Optically-stimulated luminescence (OSL) dating

OSL analysis uses luminescent emissions from quartz grains to measure time elapsed since the last light exposure for a sample, which makes it particularly useful in aeolian environments where the last light exposure represents the date of deposition and incorporation in the subsurface (Aitken, 1998; Singhvi and Porat, 2008; Forman et al., 2009). OSL-derived dates have been used in several studies examining environmental histories in the Great Plains (Stokes and Swinehart, 1997; Goble et al., 2004; Forman et al., 2005; Halfen and Johnson, 2013) and other aeolian and coastal environments (Arbogast and Muhs, 2002; Hesp and Martinez, 2007; Thomas and Wiggs, 2008; Clemensen and Murray, 2009), and have yielded OSL ages consistent with ^{14}C ages and historic observations (see Forman et al., 2009).

Single aliquot regeneration (SAR) protocols (Murray and Wintle, 2003; Wintle and Murray, 2006) were used in this study to estimate the

apparent equivalent dose of the 150–250 μm quartz fraction for 33 to 34 separate aliquots (Table 1). Each aliquot contained approximately 10 to 50 quartz grains corresponding to a 1.5 to 2.0-mm circular diameter of grains adhered (with silicon) to a 1 cm diameter circular aluminum disc. The sands analyzed were mineralogically mature with SiO_2 content of 70% to 90% of the non-carbonate fraction and are predominantly (> 80%) well-sorted quartz grains. The quartz fraction was isolated by density separations using the heavy liquid Na–polytungstate, and a 40-minute immersion in HF (40%) was applied to etch the outer ~10 μm of grains, which is affected by alpha radiation (Mejdahl and Christiansen, 1994). Quartz grains were rinsed finally in HCl (10%) to remove any insoluble fluorides. The optical purity of quartz separates was tested by exposing aliquots to infrared excitation (1.08 W from a laser diode at 845 ± 4 nm), which preferentially excites feldspar minerals. If these tests indicated feldspar contamination, the hydrofluorosilicic acid soaking was repeated. All resultant samples showed weak emissions (< 400 counts/s) with infrared excitation at or close to background counts, and the ratio of emissions from blue to infrared excitation of > 20, indicating a spectrally pure quartz extract (Durcan and Duller, 2011).

An Automated Risø TL/OSL–DA–15 system was used for SAR analyses (Bøtter-Jensen et al., 2000). Blue light excitation (470 ± 20 nm) was from an array of 30 light-emitting diodes that deliver ~15 mW/cm^2 to the sample position at 90% power. Optical stimulation for all samples was completed at an elevated temperature (125 °C) using a heating rate of 5 °C/s. All SAR emissions were integrated for the first 0.8 s of stimulation out of 40 s of measurement, with background emissions integrated for the last ten seconds of data collection, for the 30 to 40 s interval. The luminescence emission for all quartz fractions showed a dominance of a fast component with > 90% diminution of luminescence after 4 s of excitation with blue light of a fast component with > 90% diminution of luminescence after 4 s of excitation with blue light (Fig. 3). The fast ratio component was calculated for natural emission and the equivalent emissions for a regenerative dose for each aliquot as specified in Durcan and Duller (2011). Aliquots with a fast ratio of < 20 as suggested by Durcan and Duller (2011) were removed from the final equivalent dose analysis. Only 4 such aliquots were removed from population 203 aliquots (Table 1).

A series of experiments was performed to evaluate the effect of preheating at 160, 180, 200, 220, and 240 °C on isolating the most robust time-sensitive emissions and thermal transfer of the regenerative signal prior to the application of SAR dating protocols. These experiments entailed giving a known dose (2 Gy) and evaluating which preheat resulted in recovery of this dose. There was concordance with the known dose (2 Gy) for preheat temperatures above 160 °C with an initial preheat temperature used of 180 °C for 10 s in the SAR protocols. A second “cut heat” at 180 °C for 10 s was applied prior to the measurement of the test dose. A final heating at 260 °C for 40 s was applied to minimize carryover of luminescence to the succession of regenerative doses (Table 1). A test for dose reproducibility was also performed following procedures of with the initial and final regenerative dose of 4.2 Gy (Fig. 3).

The SAR protocols were used to resolve equivalent dose for six samples (Table 1). The statistical significance of an equivalent dose population was determined for 33 to 35 quartz aliquots/sample (Table 1). Aliquots were removed from analysis if the recycling ratio was not between 0.90 and 1.10, the zero dose was > 5% of the natural emissions or the error in equivalent dose determination was > 10%. Equivalent dose (D_e) distributions were log normal and exhibited overdispersion values between 13 and 60. An overdispersion percentage of a D_e distribution is an estimate of the relative standard deviation from a central D_e value in context of a statistical estimate of errors (Galbraith and Roberts, 2012). A zero overdispersion percentage indicates high internal consistency in D_e values with 95% of the D_e values within 2 sigma errors. Overdispersion values < 20% are routinely assessed for small aliquots of quartz grains that are well solar reset, like far-traveled aeolian and fluvial sands (e.g. Olley et al., 2004; Forman et al., 2014) and this value is considered a threshold metric for calculation of a D_e value using the central age model in (Galbraith and Roberts, 2012). Overdispersion values > 20% may indicate mixing of grains of various ages or partial solar resetting of grains. The minimum age model and finite mixture model are appropriate statistical treatments for such data (Galbraith and Green, 1990) and this model was used to calculate three optical ages with high > 20% overdispersion values, for the youngest sediment.

The determination of the environmental dose rate is a needed component to calculate an optical age. The dose rate is an estimate of exposure to ionizing radiation for the dated quartz grains. This value is computed from the content of U and Th, ^{40}K, Rb and cosmic radiation during the burial period (Table 1). The U and Th content of the sediments, assuming secular equilibrium in the decay series, ^{40}K, and Rb, was determined by inductively-coupled plasma-mass spectrometry by ALS Laboratories, Reno, NV. A significant cosmic ray component between 0.17 and 0.19 mGy/yr was included in the estimated dose rate taking in to account the current depth of burial (Prescott and Hutton, 1994). Moisture content (weight percent) during the burial period was inferred to 3 ± 1%, consistent with current values. The datum year for all OSL ages is 2010 CE.

4. Results

4.1. Principal Components Analysis

The PCA reveals that 99.9% of the variance on the multi-resolution dataset is contained in the first three components. Based upon a qualitative assessment of Principal Components 1, 2, and 3, it is clear the PCA identified distinct land surface geometries across the study area. Comparing individual component visualizations with a high-resolution elevation model helps identify specifically where the PCA is isolating portions of the landscape; a small creek ~25 km north of the study area provides an excellent visualization (Fig. 4). Principal Component 1 is most closely associated with flats, Component 2 is associated with convex surfaces, and Component 3 is associated with concave surfaces. The heaviest loadings of Component 1 come from creek beds, exposed bay bottoms, and several intermittently-flooded salt and mud flats. Component 2 highlights areas with a convex slope like the profile of a dune. Component 3 highlights areas dominated by more concave slopes, such as deflation flats or interdune wetlands. A composite image of Components 1, 2, and 3 stacked together shows how the relationships observed between components and land surface geometry at the creek (see Fig. 4) continue to hold true in the dune system (Fig. 5). However, the output is still not discrete enough to really help plan geochronology samples. To survey the distribution of these components' weighting around the study area, we generated an unsupervised classification of Components 1, 2, and 3 (Fig. 6).

The PCA results make sense; in a region with ~10 m of elevation change over ~3500 km^2, flatter zones are going to be statistically dominant. With wind-driven bedforms dominating much of the landscape, what relief does exist will probably be convex in profile, leaving the concavities for leftovers. Collectively, these three geometries dissect the landscape into flats, hills, and valleys. When compared to basic soil order maps of the study area (Fig. 7), the texture of the classification output clearly mimics the boundary between younger aeolian soils (inceptisols) and older, weathered surfaces (alfisols). XRF analysis of field-collected cores corroborates this conclusion. A qualitative comparison demonstrates the classification correlates well with elevation, vegetation, and soils (see Figs. 4–7).

4.2. X-Ray Fluorescence (XRF) scanning

Three focus areas demonstrate both aeolian and non-aeolian morphometries, based upon the PCA classification, and two soil cores were

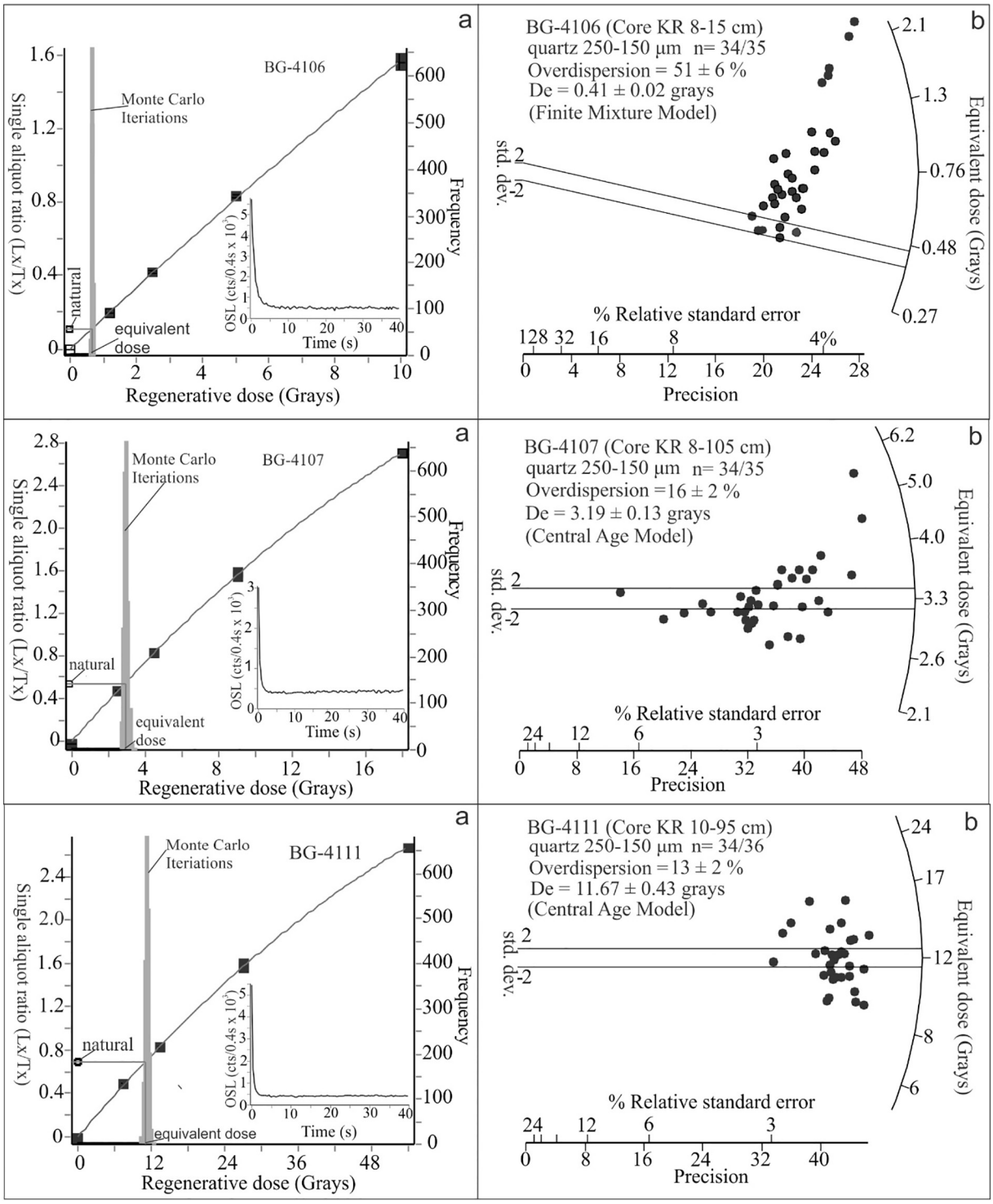

Fig. 3. a) Representative regenerative dose growth curves, with inset figure showing representative natural shine down curve b) Radial plots of equivalent dose values on small aliquots (2-mm plate of 150–250 µm quartz fraction grains).

collected from each. XRF data reveal strong associations between PCA output texture and soil characteristics across the study area. There are three soil orders across the study area; entisols, inceptisols, and alfisols. The entisols are dominated by the Falfurrias series, a hyperthermic typic ustipsamment featuring multiple buried A horizons within 1 m of the surface. The dominant inceptisols are the Topo and Cayo series, a hyperthermic typic halaquept. The alfisols are dominated by the Sarita and Nueces series, a hyperthermic grossarenic paleustalf. Within this landscape, entisols tend to dominate high-relief sandy areas like remnant knobs and sand hills. Inceptisols tend to occur near the Entisols, but along lower-slope areas like dune slacks or sand sheets. Alfisols occur in the dense oak-mesquite motte and low-lying seasonal wetlands among the grasses. Based upon the relationships between major soil orders across the study area, we expect the soil orders (and therefore geomorphic position of OSL samples) are related to time elapsed since dune stabilization.

Sites exhibiting little horizonation occur in areas with more evidence of recent aeolian processes (e.g. remnant knobs, nebkha, dust),

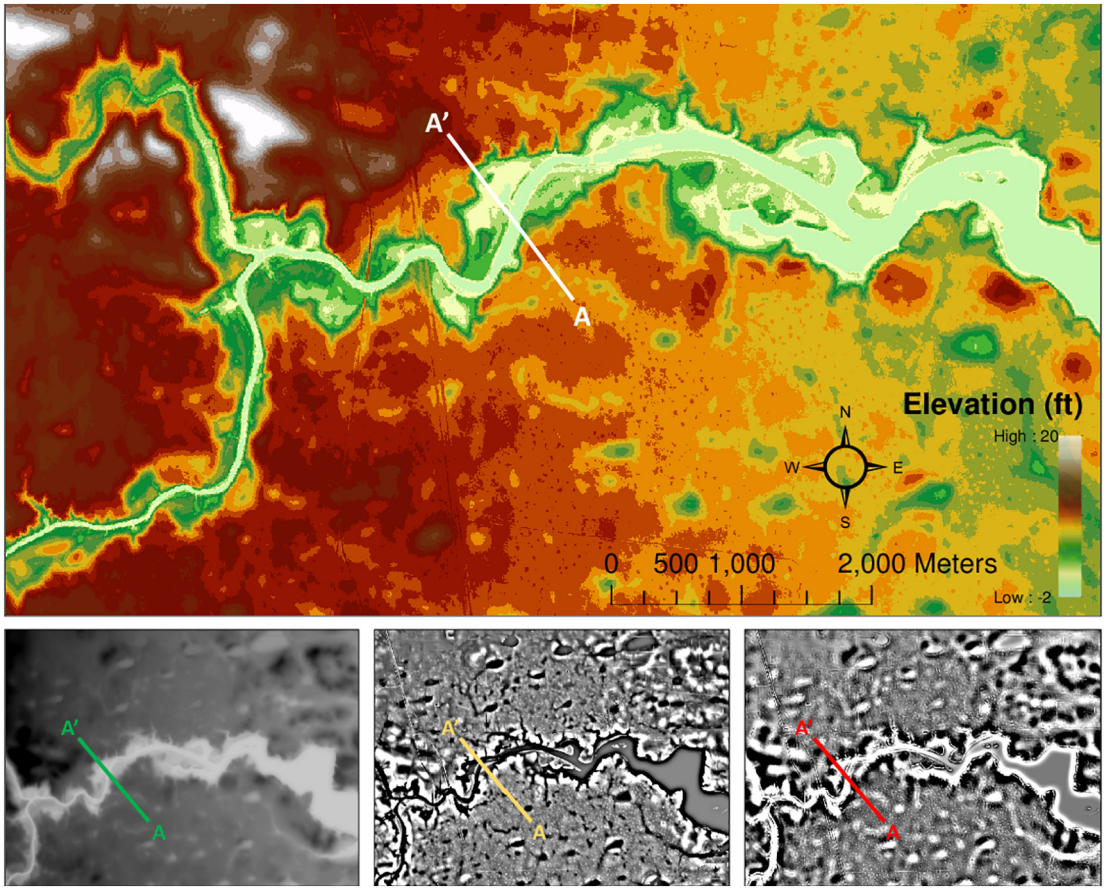

Fig. 4. Visualizations of Principal Components 1 (bottom left), 2 (bottom center), and 3 (bottom right) with an elevation model (top) to help visualize land surface geometries identified by the PCA. We selected a creek bottom – as opposed to a dune – as a sample site because it is a single, clear morphological feature where PCA results can be directly associated with specific environments. In the lower set of figures, brighter features are more heavily-weighted. PC 1 highlights the flat creek bed and bay bottom, PC 2 highlights the convex bluff tops along the creek's boundaries, and PC 3 highlights the concave banks at the base of the creekside bluffs.

and are correlated with local entisols (Falfurrias series). Sites along the margins of recently active dunes show more enhanced horizonation and are usually inceptisols (Topo and Cayo series). Sites located in topographically featureless areas with extensive woody vegetation exhibited the most horizonation and are identified as alfisols (Nueces and Sarita series).

Focus Area 1 (Cores 1 and 2, Fig. 8) is located along a sharp gradient in surface roughness and soils associated with the border between older

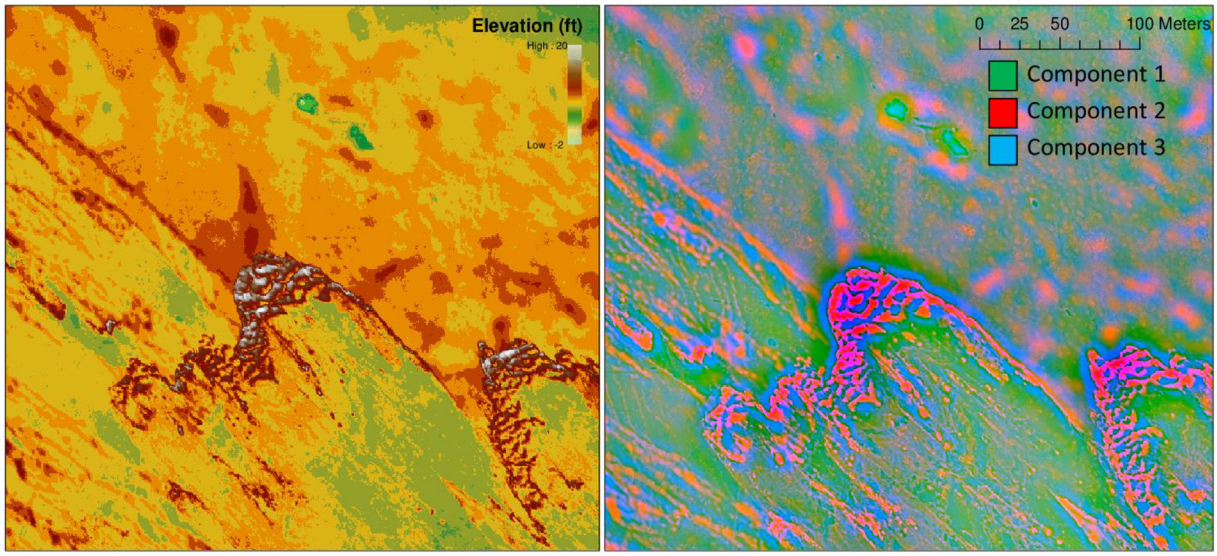

Fig. 5. Visualizations of Principal Components 1 (left), 2 (bottom), and 3 (right) with an elevation model (top) to help visualize land surface geometries identified by the PCA. In the lower set of figures, brighter features are more heavily-weighted. PC 1 highlights the flat creek bed and bay bottom, PC 2 highlights the convex bluff tops along the creek's boundaries, and PC 3 highlights the concave banks at the base of the creekside bluffs.

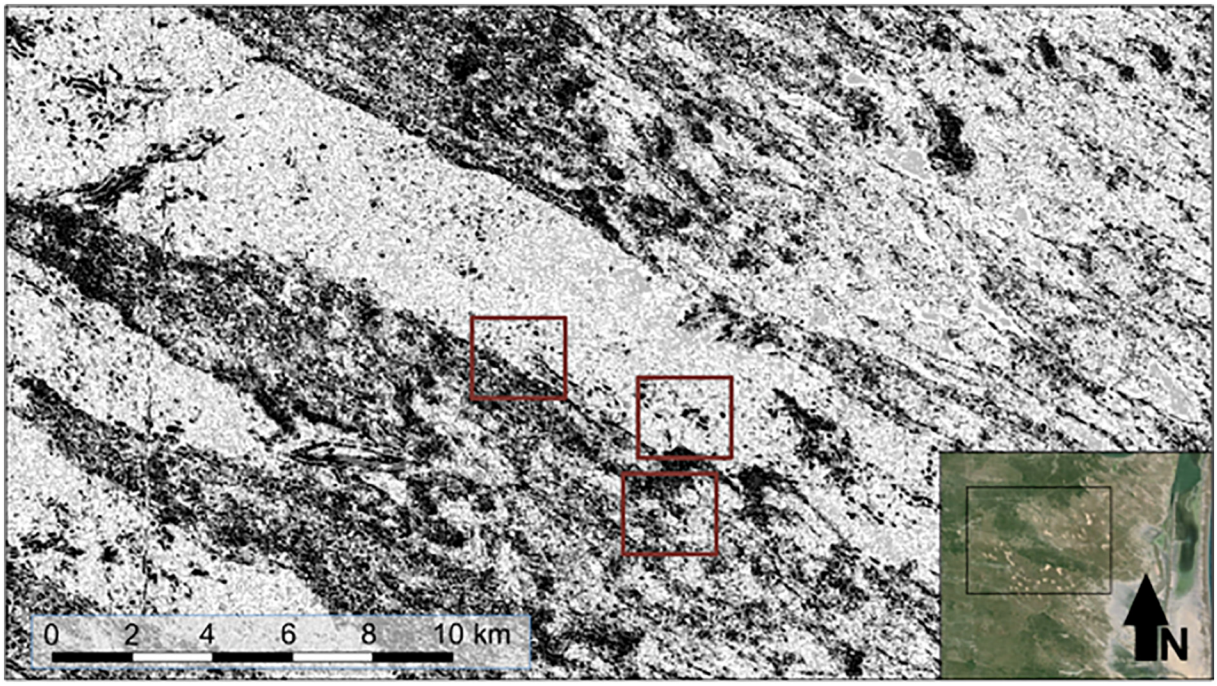

Fig. 6. Classification of Components 1, 2, and 3 with darker shades of grey indicating heavier weighting from Components 2 and 3 (e.g. more characteristically aeolian morphometries); location within the region shown as inset. There are several phases of activity evident from this image. Focus areas 1, 2, and 3 are shown with maroon boxes. (For interpretation of the references to color in this figure legend, the reader is referred to the web version of this article.)

and younger generations of dunes. Core 1 is situated just outside the area of more recent dune activity, while Core 2 is located along a dune ridge. XRF results show elemental intensities in Core 1 of Ca, Si, and Fe all change > 50% within 1 m of the surface, while Core 2 has very little change at all in elemental intensities. Similar patterns were observed in the second Focus Area (Cores 5 and 10, Fig. 9) as well as the third (Cores 9 and 6, Fig. 10). In each case, cores taken within zones classified as non-aeolian by the PCA output contain decreases in Si intensity of 20–30% within 20–120 cm of the surface. The decrease in Si intensity is accompanied by an increase in Ca and Fe intensities. Cores taken

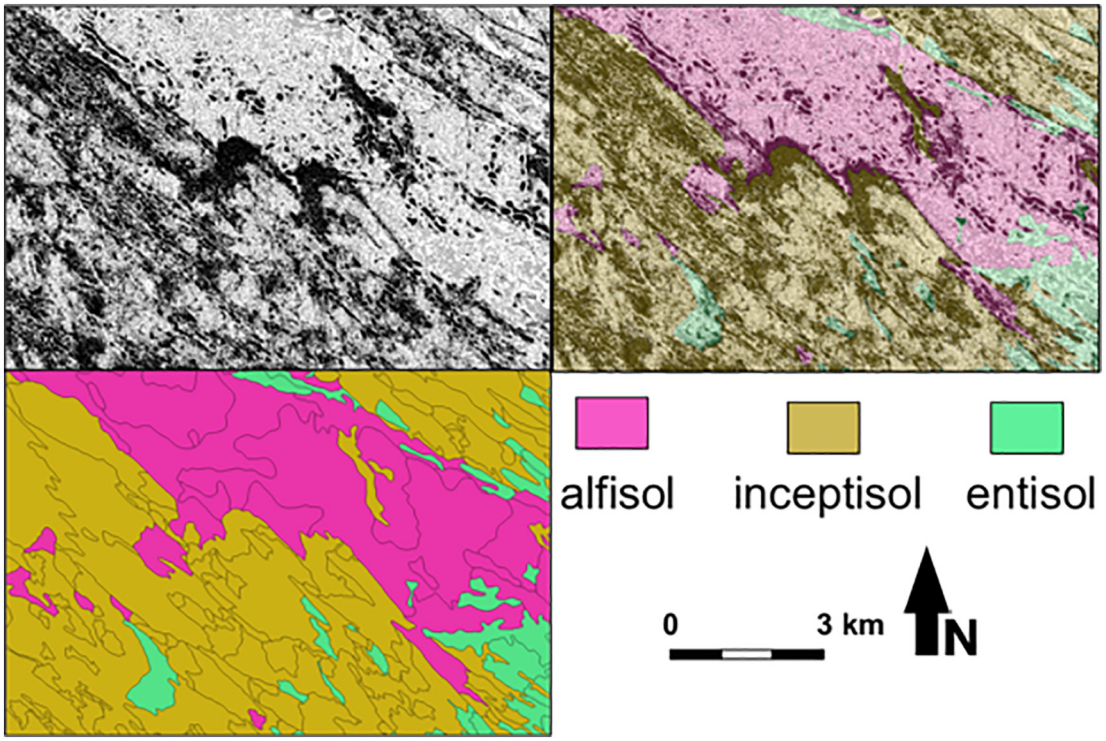

Fig. 7. Overlay (top right) of PCA classification (top left) and soil orders (bottom left) across study area. Brighter areas within the classification are less likely to be aeolian in nature, while darker areas are (according to the PCA-classification method) more likely to be aeolian. Alfisols are the most developed, inceptisols are virtually undeveloped, and entisols are at an intermediate phase of horizonation. Notice the spatial relationship between patterning in the PCA classification and major soil orders indicating age elapsed since formation began.

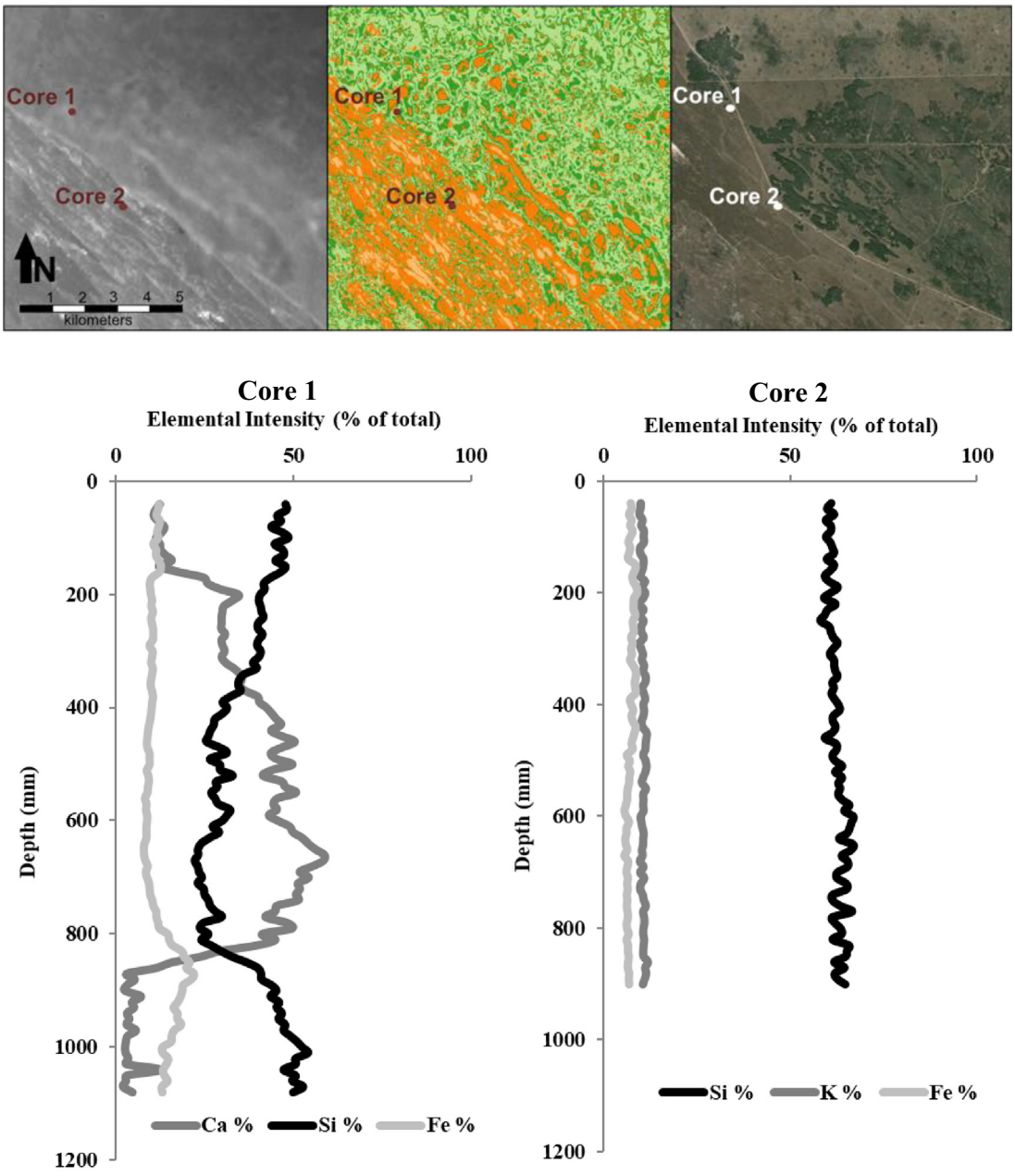

Fig. 8. Focus Area 1. Elevation model (left), PCA classification (center), and true color imagery (right). In center panel, orange areas are classified as 'aeolian' while green areas are classified as 'non-aeolian'. (For interpretation of the references to color in this figure legend, the reader is referred to the web version of this article.)

within zones classified as aeolian by the PCA output do not show changes in elemental intensity of > 10%, and show a very slight increase in Si content with increasing depth.

In Focus Area 2, there is an actively migrating dune system in the south and low, densely wooded oak motte to the north. The PCA classification recognizes the border between the active dunes and wooded flats, and areas with low undulating topography within the flats (Fig. 9). Core 5 is placed directly along a series of these features that resemble a parabolic arc – possibly a relict dune ridge. At first glance of the elevation model or in the field, these 'ridges' would not be easily identified; they are > 50 cm tall, and stretch over ~200–300 m through dense motte. Core 10, a few kilometers northeast in an area the PCA did not recognize as characteristically aeolian, exhibits the same concentration of Ca and Fe, and illuviation of Si, within the upper 1.5 m of soils. It would appear this feature represents an intermediate-age dune form, younger than the oldest portions of the sand sheet but older than the dunes still migrating across it.

In Focus Area 3, there is hummocky topography covered in tall and mixed prairie grasses with no woody vegetation (Fig. 10). Core 6 is located within a large deflation plain sitting ~1–2 m below the bordering trailing ridges. Core 9 is on a low (< 1 m prominence within 5 km) ridge surrounded by hummocky topography. Again, the XRF results match the PCA classification; Core 6 demonstrates horizonation at ~70–90 cm depth with a flip in the intensities of Ca and Si (Si decrease and Ca increase) while Core 9 features very little horizonation.

4.3. Electromagnetic induction (EMI) surveys

The previous geochronology study of this area (Forman et al., 2009) reports the sand sheet is < 3 m thick. However, the EMI results do not suggest an obvious nonconformity within 3 m of the surface, at least within this portion of the sand sheet. Conductivity generally increases

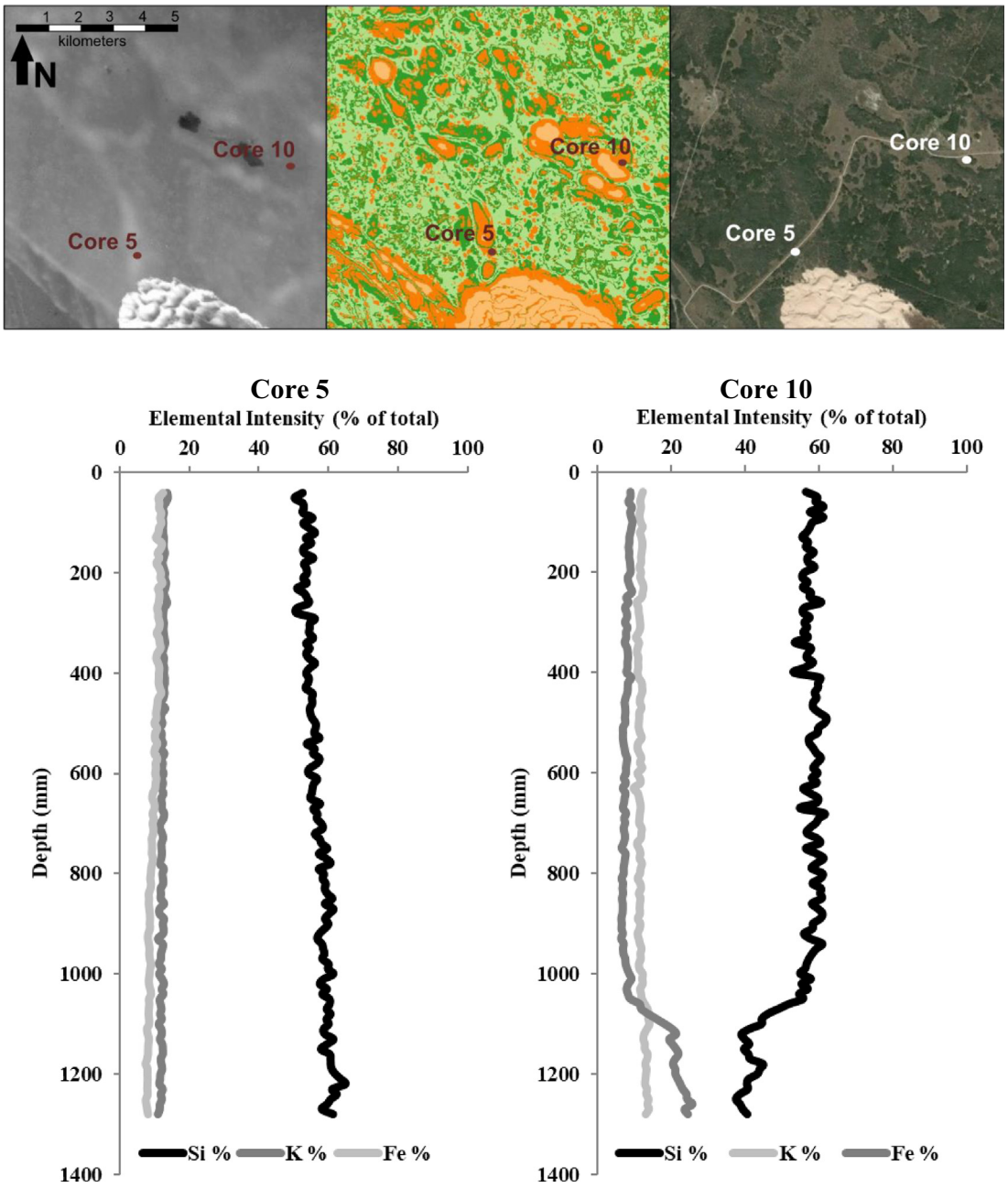

Fig. 9. Focus Area 2. Elevation model (left), PCA classification (center), and true color imagery (right). In center panel, orange areas are classified as 'aeolian' while green areas are classified as 'non-aeolian'. (For interpretation of the references to color in this figure legend, the reader is referred to the web version of this article.)

with depth across the study area from 13.4 mS/m at < 1 m to 19.8 mS/m at > 3 m and is more uniform at the surface. EMI surveys show apparent conductivity ranges from 0 to ~60 mS/m across the study area at all three frequencies. These values are consistent with observed conductivities in sandy (and perhaps silty) environments (Grisso et al., 2006; Barbosa and Overstreet, 2011).

Conductivities measured by the 15-kHz signal (within ~1 m of the surface, Fig. 11) average ~10 mS/m and are probably detecting the relatively dry, coarse dune sands mantling the surface (see Forman et al., 2009). These would be relatively non-conductive material, compared to the water-logged silts and clays logged by cores beneath the Holocene sands. The upwind (southeastern) portion of the study area is a deflation flat with elevations 1 to 2 m lower than areas downwind of the active dunes, and is noticeably more wet. A perched water table at around 70 cm depth observed near this area while collecting cores, and an artesian well feeding a livestock pond at the central-eastern margin of the study area, imply a perched water table in the shallow subsurface probably causing high apparent conductivities.

Apparent conductivity measured using 5 and 3 kHz (at ~3–4 m depth) averages 17 and 18 mS/m and varies spatially with topography. Surface morphology and vegetation communities appear related to conductivity at this depth. For instance, flat areas with woody vegetation are low-conductivity at all depths, while areas with open sand dunes are a little higher, and deflation flats upwind of active dunes are the highest conductivity.

The hot spots in apparent conductivity observed near the surface are not as continuous at lower depths and conductivities are generally higher. A large arc of lower apparent conductivities dominates the central portion of the study area, and is co-located with the dune patch seen in visible imagery at the surface. The low conductivities observed

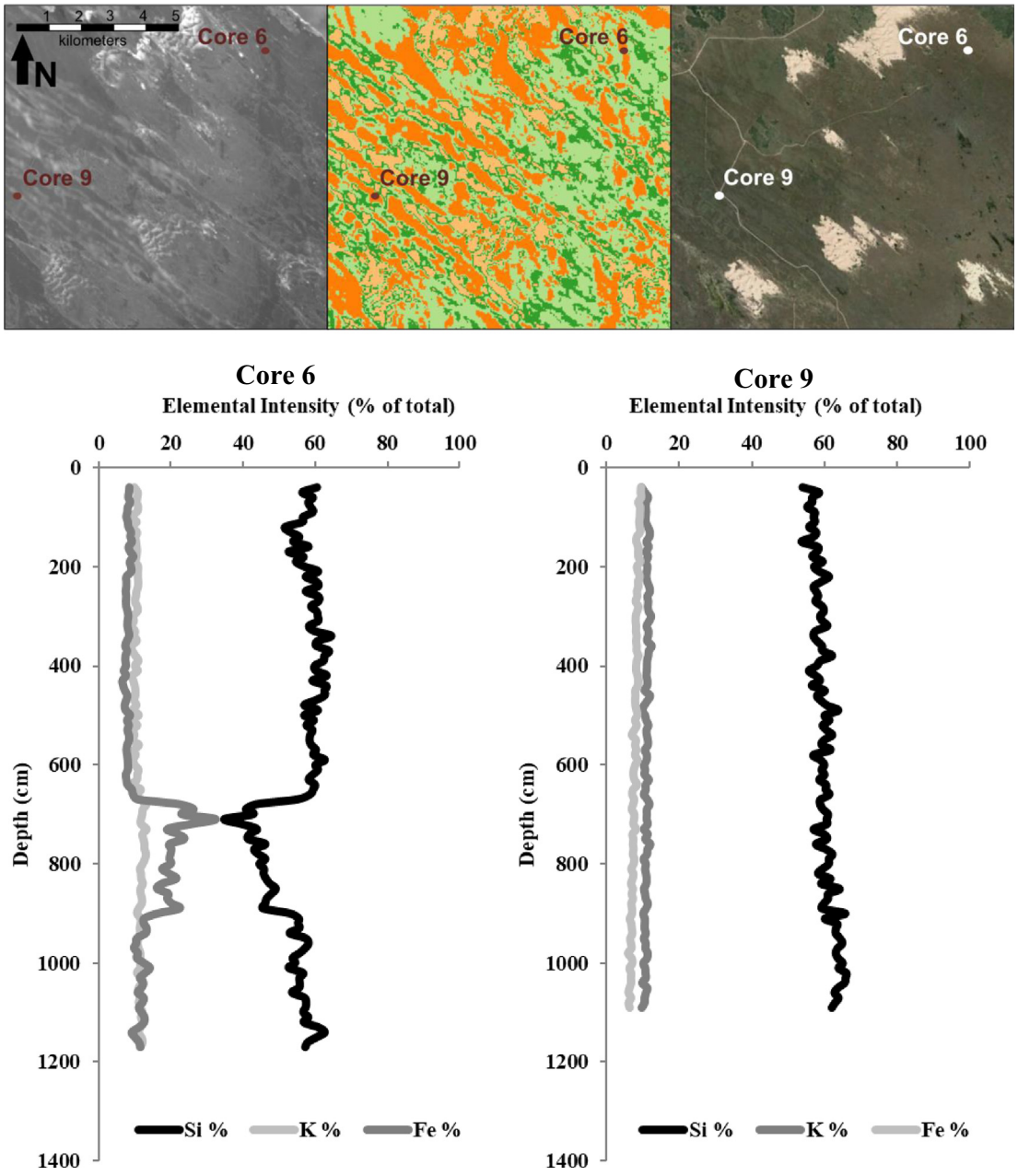

Fig. 10. Focus Area 3. Elevation model (left), PCA classification (center), and true color imagery (right). In center panel, orange areas are classified as 'aeolian' while green areas are classified as 'non-aeolian'. (For interpretation of the references to color in this figure legend, the reader is referred to the web version of this article.)

here are from the relatively coarse grain sizes found on actively migrating dunes, and the rapid infiltration capacity of aeolian sands that keeps the shallow subsurface drier than in adjacent woodlands and prairie.

4.4. Optically-stimulated luminescence (OSL) dating

Three cores were selected for OSL analysis based upon the PCA and XRF results, and the previous chronology of the STSS. Using a space for time substitution, Cores 5 and 8 are the representative members of soil characteristics on the upwind and downwind margins of actively migrating dune systems. Core 10 is used as a representative sample of much older sediments with little evidence for recent dune activity (dense woody vegetation has been in place near Core 10 for > ~80 years; Dieterle and Vera, 2015). Horizons used for sampling were selected based upon NRCS soil classification data, grain size, and elemental intensity variations representing the final stages of dune activity at the three locations (Haile and Brezina, 2012).

At Core 8, buried pale brown to brown (10YR-7/3 to 10YR-5/3) A-horizons at 15 and 40 cm probably represent humid periods where dune migration stopped between periods of relative activity (see Fig. 12). A very pale brown (10YR-7/3) C-horizon at ~100 cm most likely marks the local deflation surface for historical dune activations. The 15 cm A1-A2 contact was dated at 235 ± 20 yr, and likely represents the most recent termination of dune activity. The 100 cm A3-C1 contact was dated at 1935 ± 140 yr and probably represents the deflation surface of some previous dune activation period. Therefore, it is difficult to specify whether this sample represents the cessation of dune activity or not. At Core 5, a buried grayish brown (2.5Y-5/2) A-horizon at 15 cm depth was used as a proxy for the end of the most recent episode of aeolian activity at this site. A subtle discontinuity between B-horizons (Bknz2 and 2Bknz3) at around 100 cm depth was used as a proxy for the

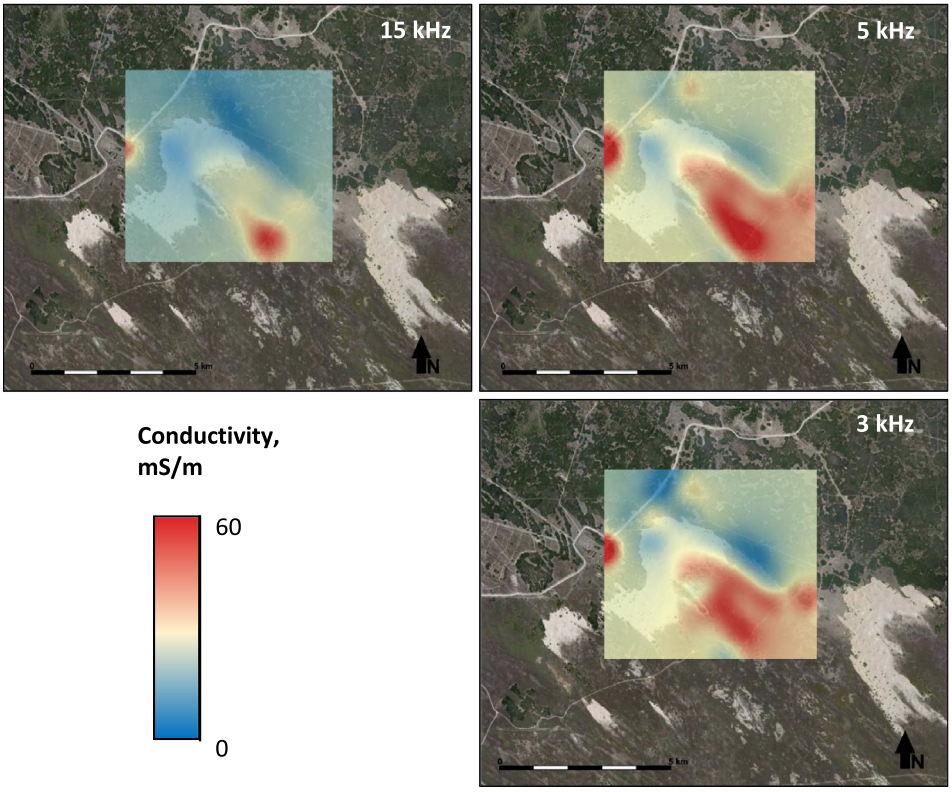

Fig. 11. Apparent conductivity survey interpolation. Higher apparent conductivities are shown in red, lower apparent conductivities are shown in blue. Measurement depths varied slightly across the study area, but averaged ~1 m at 15 kHz, ~3 m at 5 kHz, and ~4 m at 3 kHz. (For interpretation of the references to color in this figure legend, the reader is referred to the web version of this article.)

deflation surface, and initiation of dune activity. The 15 cm A1-A2 contact was dated at 75 ± 7 yr, while the 100 cm A2-2Bknz3 contact was dated at 4125 ± 300 yr.

At Core 10, an E-horizon lies between the surficial A-horizon, at roughly 35 cm depth, and discomformably above a 2Bt-horizon at roughly 95 cm depth. The A-E contact, representing the cessation of sediment deposition at the site, was dated at 230 ± 25 yr, while the E-2Bt horizon represents a relatively developed, undisturbed soil indicating no aeolian activity (therefore providing a sample beyond the oldest possible date of aeolian transport at this location) in the landscape as early as 6560 ± 460 yr.

5. Discussion

This study uses a combination of topographic, geophysical, and sedimentological data to delineate aeolian sediments on the STSS, which can then form the basis of a conceptual model of how the system interacts with climate at a millennial scale. There are two tiers of results delivered by this study. First, the survey results suggest this combined methodology may be a useful and relatively cost-effective way to characterize a relict dune system and generate a landscape history. Second, the OSL and XRF data suggest activation-stabilization patterns across the STSS are highly heterogeneous and have perhaps been occurring for much longer than previously thought.

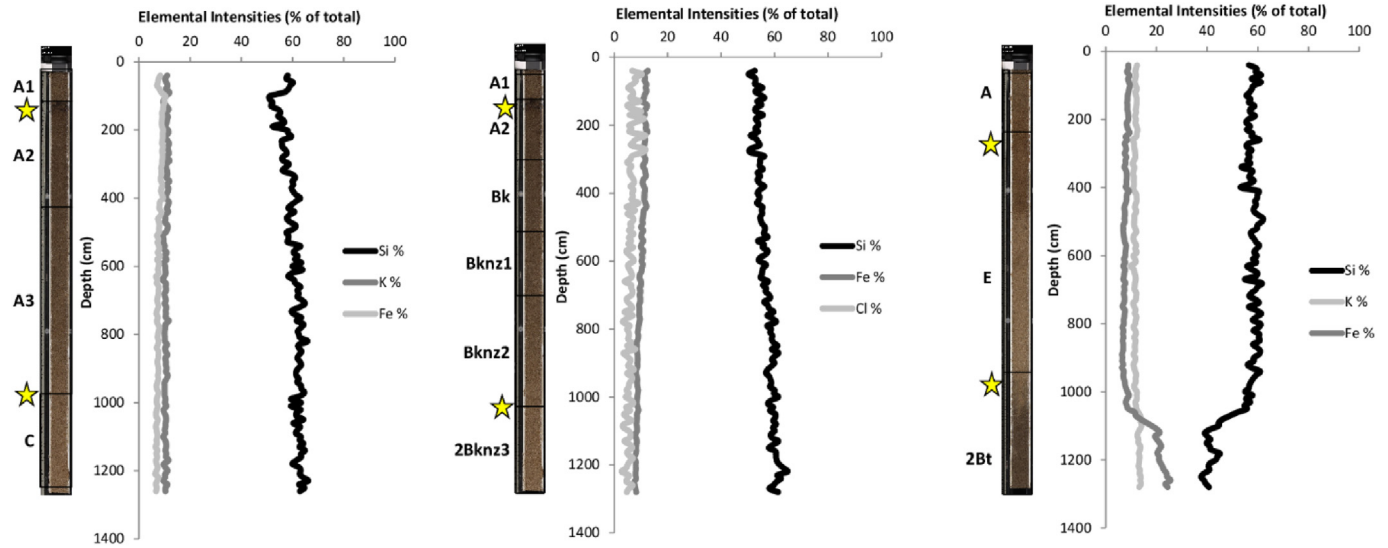

Fig. 12. Observed profile of Cores 8 (left), 5 (center), and 10 (right), shown with top three elemental intensities along with interpreted core image and location of OSL samples (shown with stars).

First, the methodological results suggest that this combination of techniques can be deployed across a relatively large area, collect continuous data series, and be used to generate detailed morphological maps across stabilized aeolian landscapes. Specifically, the PCA classification allowed for the identification of distinct morphometric signatures associated with three surface geometries (flat, convex, concave). In dunes as well as many other Earth surface systems, these geometries indicate vastly different process-form regimes. Moreover, this method identified low-relief relict dune features that OSL and XRF data confirm are > 2000 years old. The combination of methods is also able to identify where there is an absence of a preserved dune feature (e.g. ~4125 ± 300 yr sample, Core 5).

The correspondence between soils indicating distinct ages of dune activity and the PCA classification helps demonstrate the efficacy of PCA-based mapping of dune landscapes presented in Barrineau et al. (2016). The PCA generates a time series, or data cube, of elevation values calculated at different scales for each pixel. Viewed this way, similar morphometries occurring at different scales are distinct features. An incipient barchan dune and barchanoid ridge are different; one can be < 1 m tall, the other can be kilometers from side to side. Using PCA on the raw LiDAR elevation model would certainly highlight the 1-m dunes, but would have difficulty recognizing the larger landform on which individual dunes are superimposed. With the scale-dependency built into this PCA, both features can be identified as statistically distinct. This allows us to treat a single DEM as a time series, with layers of information representing larger and larger-scale measurements of average elevation. Running these layers through a k-means classification, the algorithm treats layers as it would bands of satellite imagery. In other words, this method can generate a spectral signature for distinct landforms; it automates morphological mapping.

The EMI surveys were based on the PCA classification and provided an improved picture of subsurface variations in grain size. There is an association between aeolian sands and low conductivities, likely because dune sands are generally drier and coarser than the relatively fine grains that tend to settle around vegetation. The apparent conductivities measured at ~1 m depth (15 kHz) vary only slightly and bear little resemblance to observed changes in topography and soils at the surface (see Fig. 11). The upwind (southeastern) portion of the study area is a deflation flat with elevations 1 to 2 m lower than areas downwind of the active dunes, and is noticeably more wet. A perched water table at around 70 cm depth observed near this area while collecting cores, and an artesian well feeding a livestock pond at the central-eastern margin of the study area, imply a shallow water table probably causing high apparent conductivities.

The hot spots in apparent conductivity observed near the surface are more conductive and more discontinuous than at lower depths. A large arc of lower apparent conductivities dominates the central portion of the study area, and is associated with the migrating dune patch seen in visible imagery. The low conductivities observed here are from the relatively coarse grain sizes found on dunes, and the rapid infiltration capacity of sands (relative to silts and clays) that keeps the shallow subsurface drier than in adjacent woodlands and prairie. Some areas flipped between the 3 and 15 kHz surveys; that is, they switched between relatively high and relatively low conductivities. There are two potential interpretations of this change. First, vegetation communities regularly interact with groundwater hydrology in sedimentary (non-bedrock) landscapes. The prairie and woodland vegetation (tall grasses and honey mesquite) located around the study area can access groundwater several meters laterally and vertically into the subsurface, and could be drawing water away from the dune ridges (Weaver and Zink, 1946; Nippert et al., 2011). Honey mesquite can adjust root growth patterns and depths to maximize water use during both humid and arid periods, and can affect groundwater availability for native live oaks and prairies (Ansley et al., 1991).

The second possible interpretation is related to geological framework. Previous research on the STSS suggests the Holocene aeolian sands dominating the modern surface are mantled upon Pleistocene alluvium featuring a large fluvial network (Price, 1958; Fisk, 1959; Bernard and Leblanc, 1965; Russell, 1981). This Pleistocene material varies in depth between ~2–3 m and over 8 m beneath the surface (Fisk, 1959; Forman et al., 2009). The variations in depth of the Holocene sands overlying Pleistocene alluvium may be related such that Holocene aeolian sands may have filled the topographic lows left by the Pleistocene fluvial network, a process that has been observed through exploratory cores and seismic surveys on the Laguna Madre tidal flats adjacent to the STSS (see Fisk, 1959). Modern wells drilled for fresh water are routinely in excess of 150 m depth in order to bypass smaller or more saline aquifers, so these activities almost certainly bypass the Pleistocene material and access a much deeper deposit (Dieterle and Vera, 2015, pers. comm.). Between these deeper, more substantial aquifers and the modern surface are a series of smaller aquifers and aquicludes with multiple perched water tables. The distributions of these smaller features could easily be affected by the spatial distributions of relict fluvial channels in the subsurface, particularly at depths of < 3 m (within the depth range of this study). Therefore, the variations in grain size among the Pleistocene alluvium and differential deposition of aeolian sands above it may result in a series of fragmented, localized aquifers affected below by the distribution of relict stream beds and above the rates of infiltration determined by variations in aeolian sediments. While the 3-kHz survey is only measuring apparent conductivity at ~3–4 m depth, it is possible that the groundwater dynamics in this area are affected by the geological framework underlying the modern dune surface.

It is important to note that the surveys needed to collect the EMI data took ~16 h of vigorous fieldwork to complete and did not reveal much beyond what was already apparent from the PCA analysis. Moreover, the equipment was difficult to operate in the field (any nearby buried metal objects would disrupt data collection), and the average 'cell size' for each observation (< 1 m^2) was too small to be worthwhile for surveying across dozens of square kilometers. This method is not recommended for use across a larger study area with difficult accessibility. While EMI surveys represent a great tool for examining sub-surface properties without collecting physical samples, more research is needed to fully understand linkages between surface and sub-surface processes before conductivity data can be used conclusively in this environment. The PCA classification of the landscape should be used as a guide for limited (and costly) EMI and core sampling.

Second, the OSL and XRF results suggest the South Texas Sand Sheet is much older than previously thought. OSL dates range from ~75 to ~6500 yr within ~3 m of the surface. The older samples (e.g. ~1900–6500 yr) are beyond previously published estimates for the STSS, and if they can be matched by another study suggest the need for a new conceptual model of how Padre Island and the STSS formed (see Fisk, 1959; Anderson et al., 2016).

Placing the core results in the context of the aeolian features identified through the PCA, allows for an improved interpretation of the identified structures and dates. As expected based on the PCA results, the oldest samples were collected in Core 10, and are 6560 ± 460 years old. Core 8 is the youngest, at ~1935 yr while Core 5 was last exposed ~4135 yr. These ages follow the expected pattern of Core 8 is the youngest, Core 10 is the oldest. The PCA and XRF results corroborate with OSL dates ranging from ~1900 to ~6500 yr more readily than with those ranging from ~75 to ~235 yr. This suggests the features detected by the PCA and used to identify aeolian and non-aeolian landforms range from ~1900 to 6500 years old. Specifically, Core 5 contained the youngest sample (75 ± 7 yr), while 8 and 10 were indistinguishable (235 ± 20 and 230 ± 25 yr, respectively; see Table 1). The younger sample from Core 5 may have been influenced by the construction of an access road some time before 1952 (Fig. 13).

The youngest ages are likely closely aged because much of the landscape was activated by a severe drought during the 18th century

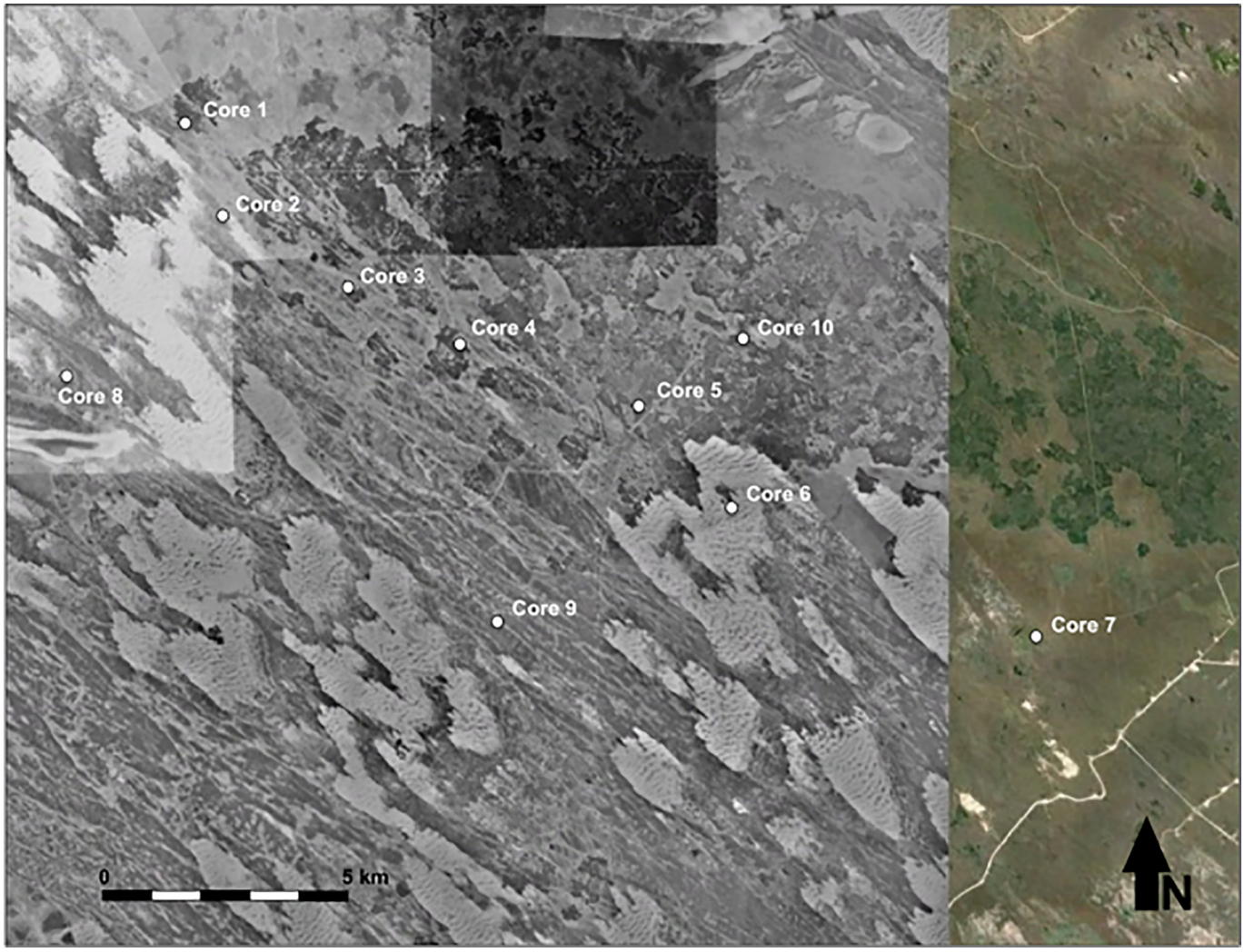

Fig. 13. Historic extent of sand dune coverage across the study area (1952). Oak-mesquite 'motte' was well-established in a belt of dense woodlands across the study area (darker shades in image). Migrating dunes were relatively more widespread than today.

(see Forman et al., 2009). This same drought led to widespread dune activation across the Texas and Oklahoma panhandles (Holliday, 1997; Frederick, 1998; Grissino-Mayer, 1996; Hall and Penner, 2012), central Great Plains (Miao et al., 2004; Halfen et al., 2010; Grimm et al., 2011; Halfen and Johnson, 2013), and even north into the Canadian prairie (Hugenholtz et al., 2012; Wolfe et al., 2006; Hugenholtz and Wolfe, 2005a, 2005b; Wolfe et al., 2000; Vance et al., 1992). The degree to which South Texas was affected by drought in the 1700s or not warrants further examination; although across much of the STSS human activity was minimal during this period, there may be some areas of anthropogeomorphic soils. Colonial records do not indicate excessive dryness (O'Shea, 1935; Berlandier, 1980; Lehmann, 1984; Fulbright et al., 1990; Jackson, 2000), however this would have been just as Europeans occupied the region so their observations were not appropriately contextualized. It is likely, based upon studies of similar systems and the distribution of OSL dates described here, that South Texas did experience a significant amount of dune activation in the 18th century.

To our knowledge this analysis provides the first description of how PCA, XRF, EMI, and OSL relate in a complex environment. The PCA and XRF results matched nicely, but the EMI results were less concrete. The younger/shallower OSL dates confirm portions of South Texas experienced aeolian accumulation (or deflation) within the past ~250 years. It is possible bioturbation within the past couple centuries may have affected the youngest sample (Core 5, 15 cm depth, 75 ± 7 yr) but this is impossible to confirm. The older/deeper round of OSL dates allows us to begin constructing a conceptual model of the landscape's millennial-scale evolution. Distinct phases of aeolian activity have occurred through history in different parts of the landscape; this is not a random emergent process, but rather a concentrated phenomenon that grows from erosional hotspots. There are quantitative and qualitative signs pointing to features that delineate deposits of different ages. Morphometry, identified using the PCA; soil chemistry and horizonation, identified using XRF; vegetation communities, identified in the field and on visible imagery; subsurface hydrology, examined using EMI. While the efficacy of these methods as individual techniques needs further examination, a qualitative interpretation of these data can be used to construct a conceptual model of aeolian landscape evolution going back to the middle Holocene (~6000 yr).

6. Conclusions

The multi-resolution PCA proved effective in delineating aeolian and non-aeolian environments, to the extent it could pinpoint aeolian versus non-aeolian soils within ~100 m of one another – across a dataset covering > 3000 km^2. By treating multi-resolution variations in elevation as distinct, this method constructs a 'spectral signature' for aeolian and non-aeolian environments. While it is far from perfect,

testing such a method in environments with distinct genealogies (e.g. floodplains, glaciers, barrier islands, etc.) should provide very useful, easily made morphological maps. XRF data confirmed the PCA classification by delineating different types of sediment; enhanced horizonation was exhibited by each sample the PCA identified as non-aeolian, while very little to no horizonation was exhibited by each sample the PCA identified as aeolian. OSL dates help tie these variations into the larger landscape's evolutionary history.

This study highlights the wealth of information that can be obtained from relict dune systems without having to extract and pay for dozens of samples based on a simple and limited interpretation of topography. There are several tell-tale signs of relict dunes than can be identified using a mixture of elevation models, soil maps, and geochemical analysis of soil samples. This study demonstrates the efficacy of PCA, XRF, EMI, and OSL in exploring the Holocene-scale dynamics of dune systems, and establishing conceptual frameworks to build environmental histories over the past 10,000 years.

Acknowledgements

The GIS laboratory staff at Texas A&M, in particular Jeff Olsenholler, made invaluable contributions to this research. In addition, the Kenedy Ranch Memorial Foundation, specifically Mr. William Dieterle and Mr. Homer Vera, enabled access to the study area and provided unmatched site-specific expertise. This research was funded in part by the American Association of Geographers Dissertation Research Grant Program.

References

Aitken, M., 1998. An Introduction to Optical Dating: The Dating of Quaternary Sediments by the Use of Photon-stimulated Luminescence. Oxford University Press, New York (267 pp.).
Albrecht, R., 1988. The adaptations of farmers in an era of declining groundwater supplies. South. Rural. Sociol. 7, 46–62.
Anderson, J., Wallace, D., Simms, A., Rodrigues, A., Weight, R., Taha, P., 2016. Recycling sedimetns between source and sink during a eustatic cycle: systems of late Quaternary northwestern Gulf of Mexico basin. Earth Sci. Rev. 153, 111–138.
Ansley, R., Boutton, T., Cuomo, G., 1991. Water relations of honey mesquite following severing of lateral roots: influence of location and amount of subsurface water. J. Range Manag. 43, 436–442.
Arbogast, A., Muhs, D., 2002. Geochemical and mineralogical evidence from eolian sediments for northwesterly mid-Holocene paleowinds, central Kansas, USA. Quat. Int. 67, 107–118.
Ashkenazy, Y., Yizhaq, H., Tsoar, H., 2012. Sand dune mobility under climate change in the Kalahari and Australian deserts. Clim. Chang. 112, 901–923.
Baas, A., Nield, J., 2010. Ecogeomorphic state variables and phase-space construction for quantifying the evolution of vegetated aeolian landscapes. Earth Surf. Process. Landf. 35, 717–731.
Barbosa, R., Overstreet, C., 2011. What Is Electrical Conductivity? Publication 3185. LSU AgCenter Research and Extension.
Barrineau, P., Dobreva, I., Bishop, M., Houser, C., 2016. Deconstructing a polygenetic landscape using multi-resolution analysis and LiDAR. Geomorphology 258, 51–67.
Berlandier, J., 1980. Journey to Mexico During the Years 1826–1834. Trans. Ohlendorf, S, et al. 2 vols. Texas State Historical Association, Austin.
Bernard, H., Leblanc, R., 1965. Resume of the Quaternary geology of the northwestern Gulf of Mexico province. In: Wright, H., Frey, D. (Eds.), The Quaternary of the United States. Princeton University Press, pp. 137–185.
Barrineau, P., Dobreva, I., Bishop, M., Houser, C., 2016. Deconstructing a polygenetic landscape using multi-resolution analysis and LiDAR. Geomorphology 258, 51–67.
Bhattachan, A., D'Odorico, P., Dintwe, K., Okin, G., Collins, S., 2014. Resilience and recovery potential of duneland vegetation in the southern Kalahari. Ecosphere 5.
Bøtter-Jensen, L., Bulur, E., Duller, G., Murray, A., 2000. Advances in luminescence instrument systems. Radiat. Meas. 32, 523–528.
Brena-Naranjo, J., Kendall, A., Hyndman, D., 2014. Improved methods for satellite-based groundwater storage estimates: a decade of monitoring the high plains aquifer from space and ground observations. Geophys. Res. Lett. 41.
Clemensen, L., Murray, A., 2009. The termination of the last major phase of aeolian sand movement, coastal dunefields, Denmark. Earth Surf. Process. Landf. 31, 795–808.
Coleou, T., Poupon, M., Azbel, K., 2003. Interpreter's corner – unsupervised seismic facies classification: a review and comparison of techniques and implementation. Lead. Edge 22, 942–953.
Cook, E., Krusic, P., 2004. The North American Drought Atlas. Lamont-Doherty Earth Observatory and the National Science Foundation Web page. http://iridl.ldeo.columbia.edu/SOURCES/.LDEO/.TRL/.NADA2004/.pdsi-atlas.html.
Cook, E., Seager, R., Cane, M., Stahle, D., 2004. North American drought: reconstructions, causes, and consequences. Earth Sci. Rev. 81, 93–134.
Cook, B.I., et al., 2016. North American megadroughts in the common era: reconstructions and simulations. Wiley Interdiscip. Rev. Clim. Chang. 7 (3), 411–432.
Cordova, C., Porter, J., Lepper, K., Kalchgruber, R., Scott, G., 2005. Preliminary assessment of sand dune stability along a bioclimatic gradient, north-central and northwestern Oklahoma. Great Plains Res. 15, 227–249.
Darrénougué, N., Deckker, P., Fitzsimmons, K., Norman, M., Reed, L., Kaars, S., Fallon, S., 2009. A late Pleistocene record of aeolian sedimentation in Blanche Cave, Naracoorte, South Australia. Quat. Sci. Rev. 28, 2600–2615.
Diamond, D., Fulbright, T., 1990. Contemporary plant-environments of upland grasslands of the coastal sand plain, Texas. Southwest. Nat. 35, 385–392.
Dieterle and Vera, pers. comm., 2015.
Durcan, J., Duller, G., 2011. The fast ratio: a rapid measure for testing the dominance of the fast component in the initial OSL signal from quartz. Radiat. Meas. 46, 1065–1072.
Ewing, R., McDonald, G., Hayes, A., 2015. Multi-spatial analysis of aeolian dune field patterns. Geomorphology 240, 44–53.
Fisk, H., 1959. Padre Island and the Laguna Madre flats, coastal South Texas. In: Proceedings of the 2nd Coastal Geography Conference. Louisiana Stat EUniversity, Baton Rouge, pp. 103–151.
Forman, S., Marin, L., Pierson, J., Gomez, J., Miller, G., Webb, R., 2005. Eolian sand depositional records from western Nebraska: landscape response to droughts in the past 1500 years. The Holocene 15, 973–981.
Forman, S., Nordt, L., Gomez, J., Pierson, J., 2009. Late Holocene dune migration on the south Texas sand sheet. Geomorphology 108, 159–170.
Forman, S., Oglesby, R., Webb, R., 2001. Temporal and spatial patterns of Holocene dune activity on the Great Plains of North America: megadroughts and climate links. Glob. Planet. Chang. 29, 1–29.
Forman, S., Wright, D., Bloszies, C., 2014. Variations in water level for Lake Turkana in the past 8500 years near Mt Porr, Kenya and the transition from the African Humid Period to Holocene aridity. Quat. Sci. Rev. 97, 84–101.
Frederick, C., 1998. Late Quaternary clay dune sedimentation on the Llano Estacado, Texas. Plains Anthropol. 43, 137–155.
Fulbright, T., Diamond, D., Rappole, J., Norwind, J., 1990. The coastal sand plain of southern Texas. Rangelands 12 (6), 337–340.
Fung, T., LeDrew, E., 1987. Application of principal components analysis to change detection. Photogramm. Eng. Remote. Sens. 53 (12), 1649–1658.
Galbraith, R., Green, P., 1990. Estimating the component ages in a finite mixture. Nucl. Tracks Radiat. Meas. 17, 197–206.
Galbraith, R., Roberts, R., 2012. Statistical aspects of equivalent dose and error calculation and display in OSL dating: an overview and some recommendations. Quat. Geochronol. 11, 1–27.
Galbraith, R.F., Roberts, R.G., Laslett, G.M., Yoshida, H., Olley, J.M., 1999. Optical dating of single and multiple grains of quartz from jinmium rock shelter, northern Australia, part 1, Experimental design and statistical models. Archaeometry 41, 339–364.
Griffith, G., Bryce, S., Omernik, J., Comstock, J., Rogers, A., Harrison, B., Hatch, S., Bezanon, D., 2004. Ecoregions of Texas. U.S. Environmental Protection Agency, Corvallis, OR.
Grimm, E., Donovan, J., Brown, K., 2011. A high-resolution record of climate variability and landscape response from Kettle Lake, northern Great Plains, North America. Quat. Sci. Rev. (19–20), 2626–2650.
Grissino-Mayer, H., 1996. A 2129-year reconstruction of precipitation for northwestern New Mexico, USA. In: Dean, J., Meko, D., Swetnam, T. (Eds.), Tree Rings, Environment, and Humanity. Arizona, Radiocarbon, Tucson, pp. 191–204.
Grisso, R., Alley, M., Holshouser, D., Thomason, W., 2006. Precision Farming Tools: Soil Electrical Conductivity. Virginia Cooperative Extension Publication, pp. 442–508.
Goble, R., Mason, J., Loope, D., Swinehart, J., 2004. Optical and radiocarbon ages of stacked paleosols and dune sands in the Nebraska Sand Hills, USA. Quat. Sci. Rev. 23, 1173–1182.
Grunsky, E., 2002. The application of principal components analysis to multi-beam RADARSAT-1 satellite imagery: a tool for land cover and terrain mapping. Can. J. Remote. Sens. 28 (6), 758–769.
Guitet, S., Cornu, J., Brunaux, O., Betbeder, J., Carozza, J., Richard-Hansen, C., 2013. Landform and landscape mapping, French Guiana (South America). J. Maps 9 (3), 325–335.
Guo, H., Marfurt, K., Liu, J., 2009. Principal component spectral analysis. Geophysics 74 (4), P35–P43.
Haile, N., Brezina, D., 2012. Soil Survey of Kennedy and Kleberg Counties, Texas. Natural Resources Conservation Service. For: United States Department of Agriculture.
Halfen, A., Johnson, W., 2013. A review of Great Plains dune field chronologies. Aeolian Res. 10, 135–160.
Halfen, A., Fredlund, G., Mahan, S., 2010. Holocene stratigraphy and chronology of the Casper dune field, Casper, Wyoming, USA. The Holocene 20, 773–785.
Hall, S., Penner, W., 2012. Stable carbon isotopes, C3-C4 vegetation, and 12,800 years of climate change in central New Mexico, USA. Palaeogeogr. Palaeoclimatol. Palaeoecol. 369, 272–281.
Haug, G., Gunther, D., Peterson, L., Sigman, D., Hughen, K., Aeschlimann, B., 2003. Climate and the collapse of Mayan civilization. Science 299, 1731–1755.
Hesp, P., Martinez, M., 2007. Disturbance in coastal dune ecosystems. In: Johnson, E., Miyanishi, K. (Eds.), Plant Disturbance Ecology: The Process and Response. Academic Press, pp. 215–247.
Holliday, V., 1997. Origin and evolution of lunettes on the High Plains of Texas and New Mexico. Quat. Res. 47, 54–69.
Houser, C., Hamilton, S., 2009. Sensitivity of post-hurricane beach and dune recovery to event frequency. Earth Surf. Process. Landf. 34 (5), 613–628.
Houser, C., Hapke, C., Hamilton, S., 2008. Controls on coastal dune morphology,

shoreline erosion and barrier island response to extreme storms. Geomorphology 100 (3–4), 223–240.
Houser, C., Wernette, P., Rentschlar, E., Jones, H., Hammond, B., Trimble, S., 2015. Post-storm beach and dune recovery: implications for barrier island resilience. Geomorphology 234, 54–63.
Huang, H., Rudd, J., 2008. Conductivity depth imaging of helicopter borne TEM data based on a pseudolayer half-space model. Geophysics 73, 115–120.
Huang, H., Won, J., 2000. Conductivity and susceptibility mapping using broadband electromagnetic sensors. J. Environ. Eng. Geophys. 5, 31–41.
Hugenholtz, C., Wolfe, S., 2005a. Biogeomorphic model of dunefield activation and stabilization on the northern Great Plains. Geomorphology 70, 53–70.
Hugenholtz, C., Wolfe, S., 2005b. Recent stabilization of active sand dunes on the Canadian prairies and relation to recent climate variations. Geomorphology 68, 131–147.
Hugenholtz, C., Levin, N., Barchyn, T., Baddock, M., 2012. Remote sensing and spatial analysis of aeolian sand dunes: a review and outlook. Earth-Sci. Rev. 111, 319–334.
Jackson, J., 2000. Texas by Teran: The Diary Kept by General Manuel de Mier y Teran on His 1828 Inspection of Texas. University of Texas press, Austin (272 pp.).
Jenkins, R., DeVries, J., 1970. Practical X-ray Spectrometry. Macmillan, London.
Jensen, J., 2005. Introductory Digital Image Processing: A Remote Sensing Perspective. Prentice Hall, Upper Saddle River, NJ, pp. 526.
Johnston, M., 1963. Past and present grasslands of Southern Texas and Northeastern Mexico. Ecology 44, 456–466.
Kettle, N., Harrington, L., Harrington, J., 2007. Groundwater depletion and agricultural land use change in the High Plains: a case study from Wichita County, Kansas. Prof. Geogr. 59 (2), 221–235.
Kocurek, G., Ewing, R., 2005. Aeolian dune field self-organization – implications for the formation of simple versus complex dune field patterns. Geomorphology 72, 94–105.
Kuriyama, Y., Lee, J., 2001. Medium-term beach profile change on a bar-trough region at Hasaki, Japan, investigated with complex principal component analysis. In: ASCE Coastal Sediments '01, pp. 959–968.
Kustu, D., Fan, Y., Robock, A., 2010. Large-scale water cycle perturbation due to irrigation pumping in the US High Plains: a synthesis of observed streamflow changes. J. Hydrol. 390, 222–244.
Lehmann, V., 1984. Bobwhites in the Rio Grande Plain of Texas. Texas A&M University Press, College Station.
LeHouerou, H., Norwine, J., 1987. The ecoclimatology of South Texas. In: Whitehead, et al. (Eds.), Arid Lands: Today and Tomorrow.
Lepper, K., Scott, G., 2005. Late Holocene aeolian activity in the Cimarron River valley of west-central Oklahoma. Geomorphology 70, 42–52.
Loope, D., Swinehart, J., 2000. Thinking like a dune field: geologic history in the Nebraska Sand Hills. Great Plains Res. 10, 5–35.
Mason, J., Swinehart, J., Goble, R., Loope, D., 2004. Late-Holocene dune activity linked to hydrological drought, Nebraska Sand Hills, USA. The Holocene 13, 209–217.
Mason, J., Lu, H., Zhou, Y., Miao, X., Swinehart, J., Liu, Z., Goble, R., Yi, S., 2009. Dune mobility and aridity at the desert margin of northern China at a time of peak monsoon strength. Geomorphology 37, 947–950.
Mejdahl, V., Christiansen, H., 1994. Procedures used for luminescence dating of sediments. Boreas 13, 403–406.
Miao, X., Mason, J., Swinehart, J., Loope, D., Hanson, P., Goble, R., Liu, X., 2004. A 10,000 year record of dune activity, dust storms, and severe drought in the central Great Plains. Geology 35, 119–122.
Muhs, D., Holliday, V., 1995. Evidence of active dune sand on the Great Plains in the 19th century from accounts of early explorers. Quat. Res. 43, 198–208.
Murray, A.S., Wintle, A.G., 2003. The single aliquot regenerative dose protocol: potential for improvements in reliability. Radiat. Meas. 37 (4), 377–381.
Nippert, J., Ocheltree, T., Skibbe, A., Kangas, L., Ham, J., Arnold, K., Brunsell, N., 2011. Linking plant growth responses across topographic gradients in tallgrass prairie. Oecologia 166, 1131–1142.
Norwine, J., Bingham, R., 1987. Frequency and Severity of Droughts in South Texas: 1900-1983. In: Braun, R. (Ed.), Livestock and Wildfire Management During Drought, 1986. Caesar Kleberg Wildlife Research Institute, Kingsville, TX.
Norwine, J., Bingham, R., Zepeda, R., 1978. Twentieth century semiarid climates and climatic fluctuations in Texas and Northeastern Mexico. J. Arid Environ. 1, 313–325.
Olley, J., De Deckker, P., Roberts, R., Fifield, L., Yoshida, H., Hancock, G., 2004. Optical dating of deep-sea sediments using single grains of quartz: a comparison with radiocarbon. Sediment. Geol. 169, 175–189.
Omernik, J., Griffith, G., 2014. Ecoregions of the conterminous United States: evolution of a hierarchical spatial framework. Environ. Manag. 54 (6), 1249–1266.
O'Shea, 1935. El Mesquite: A Story of the Early Spanish Settlements Between the Nueces and the Rio Grande. Texas A&M University Press, College Station (160 pp.).
Plant, N., Griggs, G., 1992. Interactions between nearshore processes and beach morphology near a seawall. J. Coast. Res. 8 (1), 183–200.
Prescott, J., Hutton, J., 1994. Cosmic-ray contributions to dose-rates for luminescence and ESR dating-large depths and long-term variations. Radiat. Meas. 23, 497–500.
Price, W., 1958. Sedimentology and Quaternary geomorphology of South Texas: Gulf Coast Association of Geologist Society. Transactions 8, 41–75.
Rodarmel, C., Shan, J., 2002. Principal component analysis for hyperspectral image classification. Surv. Land Inf. Sci. 62, 115–122.
Rothwell, G., Rack, F., 2006. New techniques in sediment core analysis: an introduction. In: Rothwell, G. (Ed.), New Techniques in Sediment Core Analysis. Geological Society, London, pp. 1–29.
Russell, J., 1981. The south Texas eolian sand sheet. In: Russell, J., Sterling, C. (Eds.), Modern Depositional Environments of Sands in South Texas. Gulf Coast Association of Geological Societies, Corpus Christi, Texas, pp. 43–46.
Singhvi, A., Porat, N., 2008. Impact of luminescence dating on geomorphological and paleoclimate research in drylands. Boreas 37 (4), 536–558.
Smeins, F., Diamond, D., Hanselka, C., 1991. Coastal Prairie. In: Coupland, R. (Ed.), Ecosystems of the World: Natural Grasslands. Elsevier, New York.
Sridhar, V., Loope, D., Swinehart, J., Mason, J., Oglesby, R., Rowe, C., 2006. Large wind shift on the Great Plains during the Medieval Warm Period. Science 313 (5785), 345–347.
Stokes, S., Swinehart, J., 1997. Middle- and late-Holocene dune reactivation in the Nebraska Sand hills, USA. The Holocene 7, 263–272.
Thomas, D., Wiggs, G., 2008. Aeolian system responses to global change: challenges of scale, process and temporal integration. Earth Surf. Process. Landf. 33, 1396–1418.
Thomas, D., Knight, M., Wiggs, G., 2005. Remobilization of southern African desert dune systems by twenty-first century global warming. Nature 435, 1218–1221.
Thorpe, J., Wolfe, S., Houston, B., 2008. Potential impacts of climate change on grazing capacity of native grasslands in the Canadian prairies. Can. J. Soil Sci. 595–610.
Vance, R., Mathewes, R., Clague, J., 1992. 7000 year record of lake-level change on the northern Great Plains: a high resolution proxy of past climate. Geology 20, 879–882.
Weaver, J., Zink, E., 1946. Length of life of roots of ten species of perennial range and pasture grasses. Plant Physiol. 21, 201–217.
Weltje, G., Tjallingii, R., 2008. Calibration of XRF core scanners for quantitative geochemical logging of sediment cores: theory and application. Earth Planet. Sci. Lett. 274, 423–438.
Wintle, A., Murray, A., 2006. A review of optically stimulated luminescence characteristic and their relevance in single-aliquot regeneration dating protocols. Radiat. Meas. 41 (4), 369–391.
Wolfe, S., Nickling, W., 1993. The protective role of sparse vegetation in wind erosion. Prog. Phys. Geogr. 17 (1), 50–68.
Wolfe, S., Muhs, D., David, P., McGeehin, J., 2000. Chronology and geochemistry of late Holocene Eolian deposits in the Brandon Sand Hills: Manitoba, Canada. Quat. Int. 67, 61–74.
Wolfe, S., Ollerhead, J., Huntley, D., Lian, O., 2006. Holocene dune activity and environmental change in the prairie parkland and boreal forest, central Saskatchewan, Canada. The Holocene 16, 17–29.
Woodhouse, C., Overpeck, J., 1998. 2000 years of drought variability in the central United States. Bull. Am. Meteorol. Soc. 79 (12), 2693–2714.
Wright, L., Short, A., Green, M., 1985. Short-term changes in the morphodynamic states of beaches and surf zones: an empirical predictive model. Mar. Geol. 62, 339–364.
Xiadong, M., Mason, J., Swinehart, J., Loope, D., Hanson, P., Goble, R., Xiaodong, L., 2007. A 10000 year record of dune activity, dust storms, and severe drought in the central Great Plains. Geology 35, 119–122.
Yu, J., Norwine, J., Bingham, R., Tebaldi, C., 2006. Potential Climatic Deterioration in Semiarid Subtropical South Texas. Web page. http://www.siue.edu/GEOGRAPHY/ONLINE/Yu06.doc.